Esterification of valeric acid and glycerol via various acidic zeolites

Applied Catalysis A, General 710 (2026) 120708

Contents lists available at ScienceDirect

Applied Catalysis A, General

journal homepage: www.elsevier.com/locate/apcata

Esterification of valeric acid and glycerol via various acidic zeolites

Rawipa Intakul [a,*], Phuoc Hoang Ho [a], Derek Creaser [a], Oleg Pajalic [b], Louise Olsson [a,*]

[a] Chemical Engineering, Competence Centre for Catalysis, Chalmers University of Technology, 412 96 Gothenburg, Sweden
[b] Perstorp Specialty Chemicals AB, 284 80 Perstorp, Sweden

ARTICLE INFO

Keywords:
Esterification
Zeolite
Valeric acid
Trivalerin
Glycerol
Heterogeneous catalyst

ABSTRACT

Biomass-derived green esters can be produced from the esterification of valeric acid and glycerol. In this work, various zeolites (ZSM-5, Y, and BEA) were examined, specifically targeting divalerin and trivalerin esters. A direct link between pore size and esterification performance was not evident. This outcome can be attributed to the combined influence of various characteristics such as acidity, hydrophobicity and mesoporous structure. Among the zeolite types tested, HZSM-5, HY, and HBEA with SiO_2/Al_2O_3 ratios of 87, 88.6, and 45.2, respectively, showed the best performance. The Y-zeolite with a SiO_2/Al_2O_3 atomic ratio of 88.6 produced the lowest amount of by-products. This sample had a combination of low acidity (indicating high hydrophobicity), the highest mesoporous area and a relatively high mesoporous volume. These balanced properties rendered Y zeolite with active acid sites that were easily accessible, and facilitated effective pore diffusion properties for both the reactants and products during the esterification of glycerol and valeric acid. This zeolite achieved complete glycerol conversion and a 52.9 % yield of divalerin and a 25 % of trivalerin at 130 °C after 6 h, using 1 wt% catalyst, a 5:1 acid-to-glycerol mole ratio, and continuous water removal. Additionally, the reusability of the zeolite was demonstrated, as the Y zeolite could be recycled four times with only a minimal decrease in glycerol conversion. Complete regeneration of the zeolite was also achieved through re-calcination. This study demonstrates that acidic commercial zeolites are a promising option for esterification processes due to their good catalytic performance, long-term stability and easy regeneration.

1. Introduction

Transitioning from petroleum to biomass feedstocks is crucial for reducing the chemical industry's environmental impact and moving toward sustainability. In addition to research efforts on biofuel production, the research community has also focused on valorizing lignocellulosic biomass and biobased waste streams into value-added products. Glycerol is one of the biomass-derived chemicals that can be used as a platform chemical to produce various solvents and specialty chemicals due to its high functionality with three -OH groups. It is cheaply available as a by-product from the biodiesel production process (10 wt%). The glycerol global market is growing and is forecasted to reach $5.1 billion by 2031 [1]. Among glycerol-derived chemicals, esters are used in the chemical industry as solvents, plasticizers, food additives, and biofuel additives. Glyceryl esters are suitable biofuel alternatives, offering a higher heating value and suitable polarity compared to n-butanol, ethanol, or methyl tetrahydrofuran [2].

Among different glyceryl esters, the research community has paid great attention to the acetylation of glycerol to form mono-, di-, and triacetin, which are used in the food additives industry [3–5]. Glycerol has also been esterified by C4-C5 carboxylic acids [6,7] as well as longer-chain fatty acids like oleic acid [8–10], palmitic acid [11], and lauric acid [9,12–15], which are present in animal fat and vegetable oils in the context of biodiesel production and upgrading. However, research investigating glyceryl valerates – esters of glycerol and valeric acid (VA) – is scarce. Valeric acid or pentanoic acid can be derived from biomass via levulinic acid (LA), another important biomass-derived platform compound. The conversion pathway from cellulose involves acid-catalyzed hydrolysis of 5-hydroxymethyl furfural (5-HMF) to levulinic acid (LA), followed by conversion of LA to γ-valerolactone (GVL) through hydrogenation, and finally to VA by ring opening [16]. The production of VAs from biomass has been reviewed elsewhere [17]. VA reacts with glycerol to produce glycerol valerate (monovalerin, MV), glycerol divalerate (divalerin, DV), and glycerol trivalerate (trivalerin, TV) as shown in Fig. 1. In addition to their use in biofuels, glyceryl esters have other applications, such as plasticizers, animal food additives, etc.

* Corresponding authors.
E-mail addresses: rawipa@chalmers.se (R. Intakul), louise.olsson@chalmers.se (L. Olsson).

https://doi.org/10.1016/j.apcata.2025.120708
Received 30 June 2025; Received in revised form 9 October 2025; Accepted 15 November 2025
Available online 17 November 2025

Esters are commonly produced industrially using strong homogeneous inorganic acid catalysts such as hydrochloric and sulfuric acids. However, the use of homogeneous catalysts presents challenges in terms of handling, storage, and regeneration due to their toxicity and corrosiveness. A shift to heterogeneous catalysts is advantageous for reducing process-related CO_2 emissions from energy and material consumption during the separation and regeneration of homogeneous catalysts. Various heterogeneous catalysts have been tested for the esterification of glycerol with different carboxylic acids, including ion exchange resins [3,4,18], zeolites [4,19–23], and metal oxides [6–8,24,25]. The hydrothermal stability of catalysts is desirable due to the presence of water during esterification. Water, an inevitable by-product formed during esterification, can hinder conversion due to thermodynamic equilibrium limitations and lead to catalyst deactivation. This is particularly problematic for acidic catalysts such as sulfated metal oxides and sulfonated carbonaceous solids, which are prone to leaching in aqueous environments [26,27]. Additionally, sulfate species can leach from sulfated zirconia in alcohol-containing reaction media at elevated temperatures (e.g., 120 °C) [28]. Although sulfonated-based catalysts contain strong acidity, their reusability remains a challenge. In this context, an ideal solid catalyst should exhibit not only high acidity, but also robust hydrothermal stability [29,30].

Zeolites are microporous, uniform aluminosilicate crystalline materials. They consist of TO_4 tetrahedral units, where T represents low electronegativity atoms such as Si and Al. These units are connected in a periodic pattern, forming a unique framework structure. Acidic zeolites are typically aluminosilicate-based, where their acidity and hydrophobicity are directly influenced by the ratio between Si and Al, expressed as Si/Al or SiO_2/Al_2O_3. Brønsted acid sites within the zeolite framework arise from the need to balance the negative charge introduced by Al^{3+} in the framework [31,32]. Zeolites are more thermally and chemically stable than sulfated metal oxide catalysts, which may suffer from leaching and stability issues in an aqueous environment [29]. Additionally, they offer the advantage of readily available precursors (Si and Al) for their synthesis compared to some metal oxide catalysts. Their hydrophobicity at a high SiO_2/Al_2O_3 ratio also makes them resistant to water inhibition. Various studies have found that low SiO_2/Al_2O_3 ratio zeolites tend to be less effective in esterification compared to those with higher SiO_2/Al_2O_3 ratios [4,12,33]. From these studies, optimizing the acidity, hydrophobicity, and pore structure of zeolites is crucial for steering ester product selectivity.

To the best of our knowledge, zeolites have not been examined as a heterogeneous catalyst for the esterification of VA and glycerol. However, zeolites have been studied for the esterification of glycerol or alcohol and short-chain acids like acetic acid [4,19–21]. Gonçalves et al. conducted a screening of solid acid catalysts for the acetylation of glycerol, testing various solid acid catalysts along with zeolites. The results showed that HUSY (SiO_2/Al_2O_3= 9) performed worse than HZSM-5 (SiO_2/Al_2O_3 = 56) in the esterification of acetic acid and glycerol. Glycerol conversion was reduced by half when using HUSY, which was suggested to be due to the lower SiO_2/Al_2O_3 ratio and hydrophilic character of the HUSY zeolite tested [4]. Various studies have investigated the heterogeneously catalyzed esterification of methanol and longer-chain fatty acids like oleic [34], linoleic acid [33,35], lauric acids and hexanoic acid [36], and for the esterification of glycerol and lauric acid [12] due to their application in biofuel production from fatty acids. Similarly, Milina et al. [37] investigated five distinct zeolite frameworks (FER, MOR, MFI, BEA and FAU) at varying SiO_2/Al_2O_3 ratios from 6 to 2000 for o-cresol and acetic acid esterification in the context of bio-oil upgrading. The authors reported a link between framework channel size and ester yield, where the large micropore BEA and FAU zeolites performed better than MFI, MOR and FER [37,38].

Though previous studies show that catalyst hydrophobicity and acidity both play vital roles in driving conversion [4,33], for longer-chain fatty acids and bulkier alcohols and polyols, catalyst pore size and structure or topology could become a significant factor in determining the selectivity and conversion [12,39]. The shape selectivity effect was demonstrated in a study by Machado et al. where Y, BEA, and MOR zeolites at varying SiO_2/Al_2O_3 ratios were tested for lauric acid (C12) and glycerol esterification [12]. The author found that BEA zeolite performed the best among the tested zeolites, followed by Y zeolite at similar SiO_2/Al_2O_3 ratios. BEA and Y zeolites' superior performance could be due to their three-dimensional pores, which allow the diffusion of molecules with larger kinetic diameter compared to the unidimensional porous MOR zeolite. Despite having a larger pore diameter, a unidimensional channel system can limit the diffusion of large molecules. However, a study by Fawaz [33] demonstrated that linoleic acid (C18) esterification with methanol by HZSM-5, which contains a smaller channel opening, was also viable but at high temperature. The study demonstrated that microporous HZSM-5 could achieve 79.8 % linoleate yield at a high reaction temperature of 180 °C [33]. The author proposed that to improve catalytic activity, zeolites with suitable hydrophobicity and acidity should be synthesized.

To summarize, little research has been done on the esterification of VA and glycerol using heterogeneous catalysts. According to our knowledge, there are only two studies available concerning the production of esters from VA and glycerol using heterogeneous catalysts, where Kaur et al. studied heterogeneous catalytic esterification of glycerol and VA [7,40] and butanoic acid [6] using sulfated iron oxide. However, they faced issues with recyclability, where after three cycles, the fractional conversion of carboxylic acid decreased from 83 % to 60 % [6]. The objective of the current work is, therefore, to develop stable solid acid catalysts for the esterification of glycerol and valeric acid. Due to the hydrothermal stability of zeolites, this study focuses on various zeolites as catalysts for this reaction. By systematically screening different zeolite frameworks and SiO_2/Al_2O_3 ratios, we seek to identify

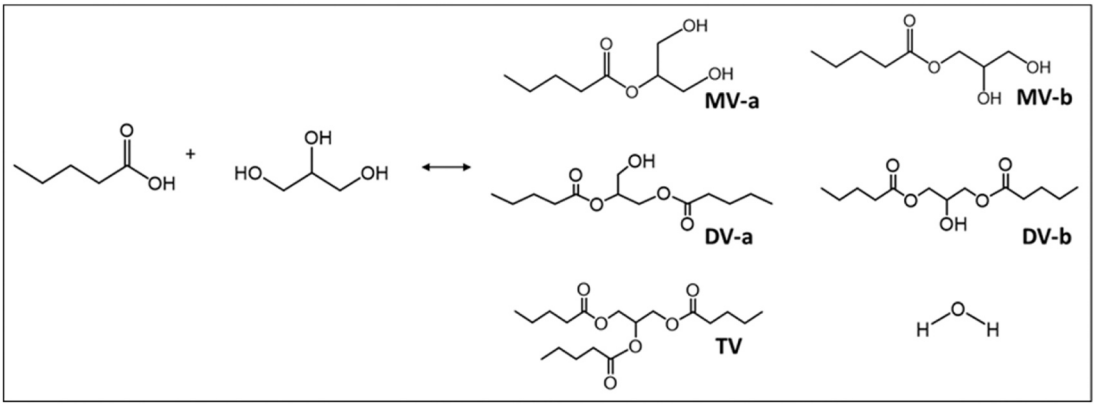

Fig. 1. Reaction products of esterification of glycerol and valeric acid (n-pentanoic acid) in the presence of acidic catalyst.

catalysts that are highly ester-selective and resistant to deactivation. The focus of the screening test in this study is on the high surface area, tailored acidity, and hydrophobicity properties of the zeolites. HBEA, HY, and HZSM-5 zeolites with varying SiO_2/Al_2O_3 ratios were studied for their pore structure, acidity, and hydrophobicity effects on selectivity toward mono -, di -, and trivalerin.

2. Materials and methods

BEA (CP814E, CP814C1 CP811C), USY (CBV300, CBV712, CBV720, CBV780), and ZSM-5 (CBV2314, CBV3024E, CBV8014, CBV28014) zeolites with different SiO_2/Al_2O_3 ratios were purchased from Zeolyst. VA (>99 %) and glycerol (>99.6 %) were obtained from Thermo Scientific Chemicals. 1-Monovalerin or 1-glycerol valerate and 1-divalerin or glycerol divalerate were purchased from Larodan AB (>98 %), and trivalerin or glycerol trivalerate was purchased from Sigma-Aldrich (>98 %). The reactants were used as received without any further purification.

2.1. Catalyst preparation and characterization

Commercial zeolites received in ammonium form were calcined in air at 500 °C for 6 h to convert them into their hydrogen form. The calcined samples were kept in a cool and dry desiccator before their use.

The textural properties were characterized by N_2 physisorption. The catalysts were degassed for 10 h under nitrogen flow at 220 °C before N_2 physisorption measurements. The N_2 physisorption was performed using a Micromeritics TriStar3000 at -196 °C. The specific surface area (S_{BET}) and pore volume (V_p) were calculated using BET (Brunauer-Emmett-Teller) [41] and single point adsorption. The total pore volume was taken at $p/p_0 = 0.99$. Micropore area (S_{micro}) and volumes (V_{micro}) were obtained from the t-plot method with the Harkins and Jura equation for curve thickness. $S_{meso/external}$ was also taken from t-plot method, where V_{meso} is taken from the difference in total pore volume and microporous volume.

Catalyst total acidity was quantified by temperature-programmed desorption of ammonia (NH_3-TPD). Approximately 30 mg of the catalyst sample was first pretreated by flowing Ar at 300 °C for 30 min, cooled to 100 °C, and kept for NH_3 adsorption. NH_3 adsorption was performed by introducing an NH_3/He (4 %) gas mixture at a 20 NmL/min flow rate for 1 h at 100 °C. After 1 h, the sample was flushed with pure Ar to remove the physisorbed NH_3 for 30 min. NH_3 desorption was done at 100 – 700 °C at a rate of 10 °C/min to desorb the NH_3. The temperature was held at 700 °C for 30 min afterward before cooling down to room temperature. The outlet gas composition was monitored by mass spectrometry (Hiden).

Pyridine adsorption measurements were performed using diffuse reflectance infrared Fourier transform spectroscopy (DRIFT) with a Bruker Vertex 70 spectrometer equipped with an MCT detector cooled by liquid nitrogen. The powder sample was packed in a stainless-steel high-temperature reaction chamber (Harrick Praying Mantis) equipped with a CaF_2 window. The measurement procedure and setup were based on a method described by de Reijer et al. [42], with minor modifications. A custom-built pyridine saturation unit was connected to the DRIFT system, enabling pyridine adsorption from a carrier gas (Ar) saturated with pyridine at room temperature. In a typical adsorption experiment, the reaction cell was first filled with inert KBr and packed with the catalyst powder. The sample was pretreated in Ar at 300 °C for 60 min following heating at a rate of 15 °C/min. A thermocouple positioned at the center of the catalyst bed monitored the temperature. Pyridine adsorption was carried out at 150 °C by exposing the sample to a 1 mL/min flow of Ar, saturated with pyridine, for 30 min. Subsequently, the sample was purged with Ar at 150 °C for 45 min to remove physisorbed pyridine. Spectra were recorded in the range of 4000–800 cm^{-1} at a resolution of 1 cm^{-1}, averaging 64 scans. The Brønsted-to-Lewis acid site ratio was determined by integrating the peaks at 1545 cm^{-1} (±25 cm^{-1}) for Brønsted sites (attributed to pyridinium ions) and at 1455 cm^{-1} (±15 cm^{-1}) for Lewis sites (attributed to pyridine coordinated to Lewis acid sites). Molar extinction coefficients proposed by Emeis [43] were used to correct the integrated areas: 1.67 cm/μmol for Brønsted and 2.22 cm/μmol for Lewis acid sites.

The SiO_2/Al_2O_3 ratio in the zeolite samples was confirmed by inductively coupled plasma (ICP-SFMS) at ALS Scandinavia AB, Luleå, Sweden, according to SS-EN ISO 17294–2:2016, US EPA Method 200.8:1994. Powder X-ray diffraction (XRD) measurements were conducted using X-ray powder diffractometer Bruker AXS D8 Advance with a 40 kV and 40 mA condition using Cu Kα monochromatic radiation source in the 2θ range of 5 ° – 60 °.

2.2. Catalytic activity test

The esterification of VA and glycerol was conducted in a 100 mL three-necked round-bottom flask equipped with N_2 flow, a gas flow meter, a temperature probe, and a reflux condenser to prevent total mass loss due to the volatility of the components. The reflux condenser outlet was connected to a gas washing bottle to trap organic vapor. In a typical esterification experiment, glycerol, VA, and the catalyst were weighed to the desired amounts and charged into a 100 mL round-bottom flask. The mixture was then stirred and heated to the reaction temperature, which took around 15 min. The time when the mixture temperature reached the target reaction temperature was regarded as reaction time 0 h. The reaction continued for a total of 6 h, with samples collected at 1 h intervals. The total reaction mixture volume was 60 mL with a starting mole ratio of VA to glycerol at 3:1, 3:2, and 5:1. The stirring speeds were set at 400 and 500 rpm, and the reaction temperatures were set at 95 °C, 110 °C and 130 °C with a control accuracy of ±1 °C. The N_2 flow rate was maintained at 15 NmL/min into the flask headspace for all experiments to keep the atmosphere inert. Catalyst loading varied between 0.5 – 4 wt% relative to the total reactant mass. Collected samples were separated from the catalyst by centrifugation and filtration. The liquid samples were stored in a cool (5–8 °C) environment before analysis by GC-MS/FID within 24 h. A mass balance based on the liquid product analysis was performed, showing a closure of 90–105 % between the total feed and products being maintained.

Catalyst reusability tests were performed by two series of experiments to investigate the effects of direct reuse, recycling with thermal treatment (calcination), and recycling with solvent washing, as shown in Scheme S1. In the first series, after the first cycle, the zeolite was recovered by centrifugation and directly reused in the next three cycles (without a washing or drying step), with additional detail for mass loss compensation in the Supplementary Information. After the fourth cycle, the spent catalyst was recovered, washed three times with ethanol, dried at room temperature for 18 h, and then calcined at 500 °C in static air for 6 h with a heating rate of 5 °C/min. This regenerated catalyst was subsequently tested for the fifth cycle. In the second series, after the first test (similar to cycle 1 in the first series), the zeolite was recovered by centrifugation, washed twice with ethanol and once with acetone, and dried at room temperature for 18 h before the next recycle test. For this series, multiple reactions were conducted for each cycle to collect enough solvent washed spent catalyst. This procedure was repeated for another three cycles. For both series, each test was performed under standard conditions: a 3-hour reaction time, 130 °C temperature, 1 wt% catalyst loading, a 5:1 molar ratio of feed acid: glycerol, reflux conditions, and 400 rpm stirring. No sampling was performed during the reaction cycles.

2.3. Liquid product and spent catalyst characterization

The liquid sample was analyzed and quantified by GC-MS/FID (Agilent 7890B-5977A) equipped with an Agilent VF-1701ms column (30 m x 250 μm x 0.25 μm) with di-n-butyl ether as an internal standard. The injection temperature was set at 280 °C. The oven temperature was

initially set at 110 °C and then heated to 280 °C. Quantification of liquid products was performed by external calibration of standard reference compounds using a flame ionization detector (FID). The following equations show the calculations of glycerol conversion, ester yields, and selectivity, respectively.

$$\text{Conversion}(\%) = \left(1 - \frac{\textit{mole of unreacted reactant}}{\textit{initial mole of the reactant}}\right)\text{x}100$$

$$\text{Selectivity}(\%) = \left(\frac{\textit{mole of product}}{\textit{mole of reacted glycerol}}\right)\text{x}100$$

$$\text{Yield}(\%) = \left(\frac{\textit{mole of product}}{\textit{mole of initial glycerol}}\right)\text{x}100$$

The water content in the liquid product was quantified using a Metrohm 870 KF volumetric Karl Fischer (KF) titrator V20. A 0.1 g liquid sample was weighed and titrated with HYDRANAL – composite 5 (Honeywell Fluka™). Three replicates of KF titration were performed and the average values of water content were used. The content of Al and Si metal species in the product liquid mixtures were determined by ICP-SFMS (ALS Scandinavia AB, Luleå, Sweden) according to SS-EN ISO 17294–2:2016 and US EPA Method 200.8:1994.

Selected ethanol-washed and dried spent catalysts were analyzed by Thermogravimetric analysis (TGA). Approximately 10 mg of spent and fresh catalysts were weighed and placed in a 70 μL alumina crucible, then put into the TGA measurement cell starting at a temperature of 40 °C. The cell was heated up to 800 °C in the presence of air flow at a rate of 5 °C/min.

The thermal regenerated catalysts were characterized by X-ray diffraction (XRD), N_2 physisorption, and scanning electron microscopy (SEM) to examine the integrity of the catalysts after reusages. The crystallography of selected fresh and regenerated spent catalysts was examined by X-ray diffraction (XRD) with diffraction angle (2θ) in the range of 5–60 °. SEM measurements of fresh and regenerated spent catalysts were conducted using a JEOL 7800 F Prime Scanning electron microscope at a 5 kV accelerating voltage. The sample for SEM measurement was loaded on the carbon tape on aluminum holder and coated with 4 nm gold using a Leica EM ACE600 high vacuum sputter coater.

3. Results and discussion

3.1. Catalyst characterization

The nitrogen adsorption-desorption isotherms at −196 °C of the zeolites studied, shown in Fig. 2, reveal distinct textural characteristics for microporous and mesoporous zeolites. The corresponding BET surface area, micropore volume, and total pore volumes are shown in Table 1. The SiO_2/Al_2O_3 ratios, as measured by ICP-SFMS, are also listed in Table 1. From N_2 adsorption and desorption isotherms shown in Fig. 2, most zeolites exhibit composite IUPAC type I and type IV(a) isotherms. HZSM5 zeolites display a steep nitrogen uptake at low relative pressure ($P/P_0<0.1$), indicating the presence of micropores, which is consistent with the microporous MFI structure. At higher relative pressures (P/P_0), the isotherms show characteristic features of mesoporous materials. These mesoporous characteristics vary depending on the zeolite framework and SiO_2/Al_2O_3 ratio. Minimal H4 hysteresis loops are observed for HZSM5–23 and 30, whereas the samples with higher SiO_2/Al_2O_3 ratios (80 and 280) display a slight increase in nitrogen uptake at higher P/P_0, suggesting the presence of interparticle porosity or minor mesopore formation. Indeed, HZSM5–80 and 280 possess higher mesopore volumes than HZSM-5 with a lower SiO_2/Al_2O_3 ratio, as listed in Table 1. In contrast, the HBEA zeolites show pronounced H4 hysteresis loops, associated with aggregated zeolites and mesoporosity. Fig. 2c presents the physisorption isotherms for the HY zeolite series. The isotherms for HY12, HY-30, and HY-80 can be classified as composite type I and IV (a). However, the isotherm for HY-5.1 corresponds to type Ia without a hysteresis loop, indicating a distinct microporous structure compared to HY with higher SiO_2/Al_2O_3 ratios. Indeed, according to Tables 1, HY-5.1 contains microporosity with limited mesoporosity compared to HY zeolites with higher SiO_2/Al_2O_3 ratios. The difference could arise from production of HY12, HY-30 and HY-80, which are ultra-stable Y (USY) zeolites produced via dealumination to obtain high SiO_2/Al_2O_3 ratio.

The analysis of acid site density and strength is crucial for understanding the catalytic performance of the zeolites. Both acid site density and relative acid site strength distribution of the commercial zeolites were measured by NH_3-TPD. Based on the total acidity in Table 1, zeolites with a high SiO_2/Al_2O_3 ratio — commonly referred to as high-siliceous zeolites — contain fewer total acid sites, as expected. This is because Brønsted acidity in zeolites originates from the isomorphous substitution of Si with Al in the framework, forming Si-O-Al-OH groups [31,32]. Fig. 3 shows the NH_3-TPD desorption profiles for the examined zeolites. Generally, two NH_3 desorption peaks were observed around 200 °C and 350–450 °C. The lower temperature desorption peak correlates to weaker acid sites, while the higher temperature desorption peak corresponds to stronger acid sites [44–46]. The interpretation and quantification of acid site strength must be done carefully as peak width and peak temperature shift can depend on experimental conditions, i.e., NH_3 adsorption temperature, carrier gas flow rate, time, the ratio between sample weight and flow (W/F), and the zeolites' intracrystalline diffusion limitation of desorbing ammonia [44,47]. The ammonia heat of adsorption is not only influenced by acid strength but also by the zeolite pore confinement steric effects [48]. For comparative purposes in this study, the distribution of acid site strength is analyzed based on the integration of NH_3 desorption peaks in the range of 100–300 °C for weak acid and 300–700 °C for strong acid sites (shown in Figure S1), rather than a direct comparison of temperature of the desorption peak. These weak and strong acid sites are assumed to correspond, respectively, to

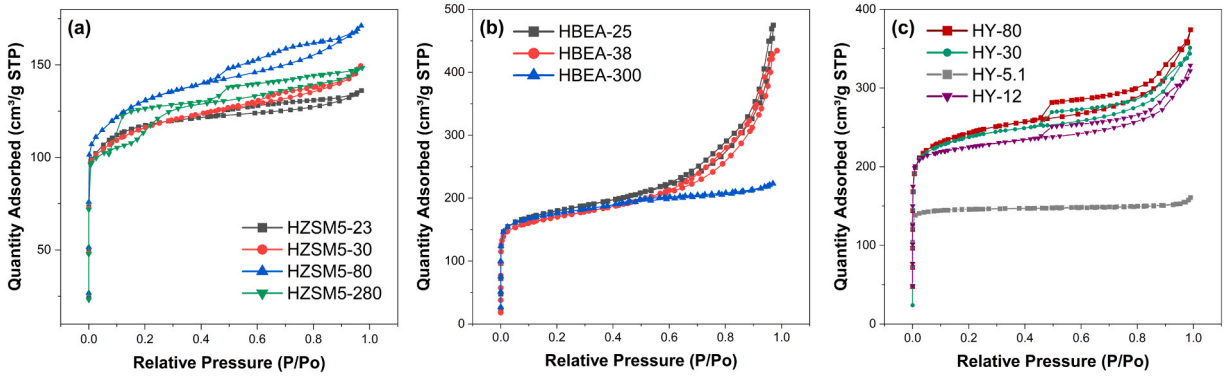

Fig. 2. N_2 adsorption-desorption isotherms for zeolites measured at −196 °C, for (a) HZSM5 (b) HBEA and (c) HY.

Table 1
Textural properties, SiO_2/Al_2O_3 ratio, and acidity characteristics of the tested zeolites.

Catalyst	Supplier Codes	SiO_2/Al_2O_3[a]	S_{BET} - specific surface area (m^2/g)	S_{micro}[b] (m^2/g)	S_{meso}[b] (m^2/g)	V_p (Total pore volume cm^3/g)[c]	V_{micro}[b] (cm^3/g)	V_{meso} (cm^3/g)	Acidity[e] (NH_3 μmol/g)
HBEA-25	CP814E	25.6	669.5	448.1	221.4	0.73	0.17	0.56	704
HBEA-38	CP814C	45.2	621.3	473.1	148.2	0.67	0.18	0.49	731
HBEA-300	CP811C	238	625.4	449.8	175.6	0.52	0.20	0.32	250
HZSM5–23	CBV2314	25.8	441.4	254.5	186.9	0.21	0.10	0.11	1362
HZSM5–30	CBV3024E	29	431.3	275.6	155.7	0.23	0.12	0.11	802
HZSM5–80	CBV8014	87	479.5	258.7	220.8	0.28	0.10	0.18	428
HZSM5–280	CBV28014	376.8	422.0	294.2	127.8	0.23	0.12	0.11	125
HY-5.1	CBV300	5.6	597.1	554.7	42.4	0.25	0.21	0.04	1176
HY-12	CBV712	12.6	870.5	697.3	173.2	0.49	0.27	0.22	729
HY-30	CBV720	35.4	820.9	590.2	230.7	0.54	0.26	0.28	495
HY-80	CBV780	88.6	808.1	548.8	259.3	0.59	0.26	0.33	187

[a] Si and Al contents quantified by ICP-SFMS
[b] Micropore surface area, mesoporous/external surface area, and volume obtained from t-plot.
[c] Total pore volume taken at $p/p_0 = 0.99$
[e] Quantified by NH_3-TPD

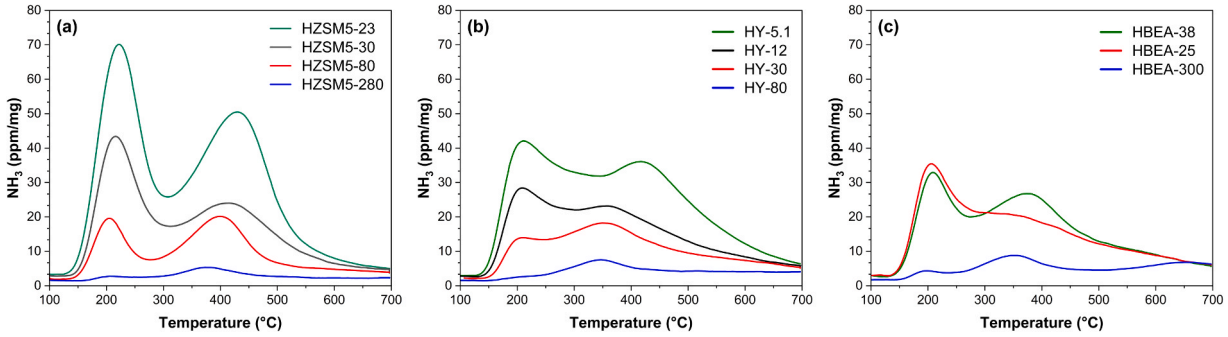

Fig. 3. NH_3-TPD desorption profile of (a) ZSM-5, (b) Y and (c) BEA zeolites.

Lewis and Brønsted acid sites, although some overlap may exist. On the other hand, the low SiO_2/Al_2O_3 zeolite contains high total acidity, as seen in Table 1 and Fig. 3. High alumina content zeolites like HZSM5–23 and HY-5.1 showed two distinct NH_3 desorption peaks with high intensities for both peaks. Whereas high siliceous zeolites like HBEA-300, HY-80, and HZSM5–280 showed mainly higher temperature desorption peaks at 350–400 °C (see Fig. 3). Another trend observed from NH_3 measurements is an increase in the proportion of strong acid sites when increasing the SiO_2/Al_2O_3 ratio, which was found for all three zeolite frameworks in this study. Figure S1 shows that more than 70 % of acid sites in HBEA-300, HY-80, and HZSM5–80 are strong acid sites

3.2. *Catalytic performance: effect of catalyst and reaction time*

The catalytic performances of zeolites were evaluated through the esterification of glycerol and n-pentanoic acid (valeric acid, VA). Three ester products (MV, DV, and TV), and water were detected in the reaction mixture. Note that the isomers of MV and DV were not individually quantified by GC-MS/FID in this study. The mass balance closure was found to be between 90 and 100 wt%. Carbon mole balances between the limiting reactant and products were found to be between 90 and 105 mol%.

The esterification between VA and glycerol can occur at a non-negligible rate without the addition of a catalyst, since esterification

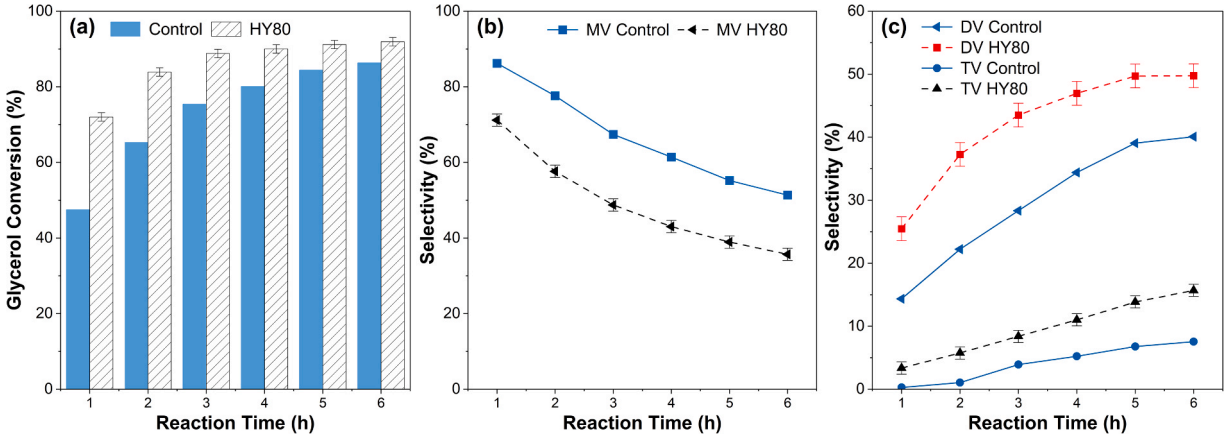

Fig. 4. The effect of reaction time for control run and HY-80 on a) glycerol conversion, b) MV selectivity, c) DV and TV selectivity. Experiments were conducted at 130 °C, 5:1 acid to glycerol mole ratio, 1 wt% catalyst loading, and 400 rpm stirring rate.

reactions can be autocatalyzed by the acid reactant [49,50]. Consequently, a control experiment without zeolites was performed under the same reaction conditions: 130°C, a 5:1 acid: glycerol mole ratio, and 400 rpm stirring rate. To assess the esterification reactivity of zeolites, the performance of a selected zeolite, HY-80, was compared to the control run in Fig. 4. To validate the results, the HY-80 experiments were repeated three times, and the standard deviation was calculated and included in Fig. 4.

With excess VA and reaction temperature of 130 °C, the results in Fig. 4 shows that the control esterification of VA and glycerol already formed MV, DV, and TV ester products without the help of solid acid catalysts. However, in the presence of HY-80, glycerol conversion and product selectivity shifted toward higher esters, DV and TV, which are more favorable as ester products, at a faster rate. As reaction time progressed, glycerol conversion increased in both the control and HY-80 experiments. For instance, after 1 h, HY-80 zeolite enhanced the glycerol conversion by 25 % compared to the control experiment, increasing it from 47 % to 72 % (Fig. 4a). TV formation began with 1–2 % selectivity during the first 2 h in the control experiment, whereas HY-80 achieved 7 % selectivity for TV with the same time frame (Fig. 4c). The significant mesoporosity of HY-80 likely contributes to an enhanced reaction rate and increased formation of the higher ester products, due to favorable diffusion effects, which will be discussed further in Section 3.3.1. These results indicate that zeolites can serve as effective solid acid catalysts, enhancing both the rate of glycerol conversion and the production of esters.

HY-80 zeolite can contain both Lewis and Brønsted acid sites that can both catalyze esterification reactions. The Brønsted acid-catalyzed esterification mechanism, known as Fischer-esterification, involves the protonation of the carbonyl group in a carboxylic acid molecule to form a carbocation. This is followed by a nucleophilic attack by the oxygen atom of the alcohol molecule, forming an oxonium ion. Subsequently, proton transfer, elimination of water, and deprotonation liberate an ester molecule. All zeolites in this study are in protonated form, therefore containing Brønsted acid sites that are active for Fischer esterification [19,51,52]. The NH_3-TPD measurements revealed that HY-80 used in this study contained a total acidity of 187 μmol/g (Table 1). Fig. 3b and Figure S1b also show the NH_3 desorption profile of HY-80, with > 80 % of its NH_3 desorption peaks in the higher temperature range (350–450 °C), indicating a predominance of Brønsted as well as possibly stronger Lewis acid sites. To better distinguish between these acid site types, pyridine adsorption infrared (IR) spectroscopy is often employed. In this study, pyridine adsorption DRIFTS measurements at 150 °C were conducted for HY-5.1, HY-30 and HY-80 (Table 2 and Figure S2). The HY-80 zeolite exhibited a prominent peak around 1545 cm^{-1} (Figure S2a), corresponding to Brønsted acid sites (BAS), while the peak at 1455 cm^{-1}, associated with Lewis acid sites (LAS), was less pronounced (Figure S2b). The Brønsted-to-Lewis acid site ratio (B/L) was calculated using the formula reported by Platon et al. [53], using molar extinction coefficients from Emies [43]. As shown in Table 2, the B/L ratio increased with decreasing Al content across the HY zeolite series (Table 2, from DRIFTS in Figure S2), consistent with the higher proportion of stronger acid sites indicated by NH_3 desorption data (Figure S1b). The calculated Brønsted-to-Lewis acid site (B/L) ratio for HY-80 was 5.17, based on 157 μmol/g of NH_3 desorbed from BAS and 30 μmol/g from LAS. (Table 2). These results align with existing literature. Morin et al. quantified Brønsted and Lewis acid sites in the commercial CBV series Y zeolite (Zeolyst) using pyridine adsorption IR at 150 °C, reporting a predominance of Brønsted acid sites, with Lewis acid site concentrations 2–4 times lower [54]. Similarly, Imbert et al. reported Brønsted acidity values of 129 μmol/g and Lewis acidity of 42.9 μmol/g for CBV780 (HY-80) under the same conditions [55]. The high B/L ratios for zeolite HY-80 may arise from the process of synthesizing CBV780 (HY-80). According to the literature, CBV780 is produced by subjecting the parent high-alumina HY to steam treatments and acid leaching [54–56]. The acid leaching process removes extra framework aluminum species, reducing the LAS concentration in the HY-80 sample. This resulting BAS content of 84 % in HY80 is consistent with the NH_3 desorption profile (Figure S1b), which indicates that more than 80 % of acid sites are strong, as evident from the high-temperature NH_3 desorption.

Additionally, zeolites are also known for their unique shape selectivity, stemming from their porous ordered network structure. In addition to the surface -OH groups, the Brønsted acid sites, stemming from the presence of aluminum and an extra framework proton attached to Si-O-Al to balance the negative charge [31,32], are mostly found inside the zeolite pore framework. The reactant molecules must diffuse inside the zeolites' pores before interacting with Brønsted acid sites that are positioned inside the framework structure as Si-OH-Al groups or silanol Si-OH-Si groups [32,57]. Our results in Fig. 4 suggest that Brønsted acid sites inside the pores of HY-80 are accessible to catalyze valeric acid and glycerol, allowing them to react and form esters. This could be aided by the mesoporosity of HY-80 (Table 1). The effect of pore morphology of different zeolite frameworks will be discussed more in S ections 3.3 and 3.5.

In terms of product selectivity and the effect of reaction time, Fig. 4b and Fig. 4c show product selectivity for MV, DV and TV at varying reaction times (1–6 h), a reaction temperature of 130 °C, and a 5:1 acid-to-glycerol feed mole ratio. At the early stage of esterification, the majority of products formed are detected and identified by GC-MS/FID as MV. As the reaction progressed, the glycerol conversion and the formation of DV and TV increased. This is expected as monovalerin is initially formed, followed by the formation of DV and TV via esterification between the remaining -OH groups in monovalerin and VA molecules (see Fig. 1). From Fig. 4a, it can also be observed that glycerol conversion, catalyzed by HY-80, approaches the thermodynamic equilibrium level at 6 h. However, the product distribution has not yet reached equilibrium, as seen in Fig. 4c, where TV selectivity is still increasing. Approaching the glycerol conversion equilibrium point at 6 h, although HY-80 improved glycerol conversion by only 6 %, the total selectivity for DV and TV by HY-80 is 18 % higher than the control run. In addition to the main valeric ester products, a small amount of side products, accounting for less than 0.5 % of the total FID area percentage, was detected in the GC-MS/FID analysis of the liquid product for both control and HY-80 runs. These side products were not identified in this study and are thus reported as FID area percentages in Table S1.

Table 2
Brønsted-to-Lewis acid site ratios for selected HY zeolites measured by Pyridine-DRIFTS adsorption at 150 °C.

Zeolites	B/L[a]	BAS (%)[a]	LAS (%)[a]	**BAS** (NH_3 μmol/g)[b]	**LAS** (NH_3 μmol/g)[b]
HY-5.1	1.62	62	38	722	445
HY-30	1.75	64	36	315	180
HY-80	5.17	84	16	157	30

[a] Integrated absorbance intensity corrected using molar extinction coefficients reported by [43].
[b] Calculated by multiplying BAS (%) from pyridine DRIFT result by total acidity from NH_3-TPD measurement.

3.3. Zeolite screening

Based on the esterification reactivity results of HY-80, it can be inferred that zeolites are effective solid acid catalysts for producing glyceryl valerate esters. We examined three types of protonated zeolites, including BEA, Y, and ZSM5, at varying SiO_2/Al_2O_3 ratios to assess their esterification reactivities. To evaluate the zeolites, glycerol conversion (%) and ester product yield (%) were determined, after a 2 h reaction time, which is far from the equilibrium point, at 130 °C, 400 rpm, and total reflux conditions. These results were compared with a control experiment without a catalyst, at the same conditions, as shown in

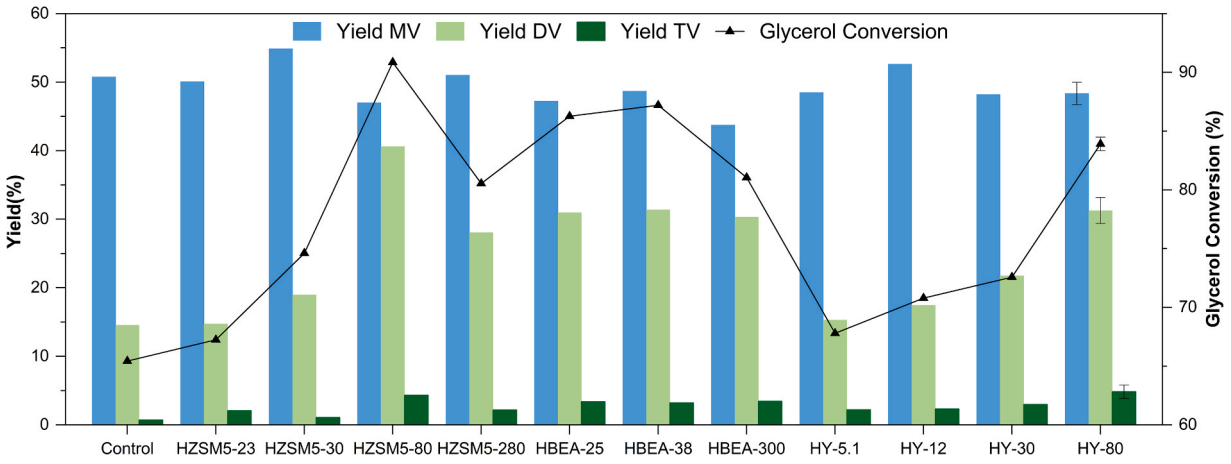

Fig. 5. Comparison between the reactivity of zeolites for esterification after 2 h at 130 °C, 400 rpm, 5:1 acid-to-glycerol mole ratio, 1 wt% catalyst loading under total reflux.

Fig. 5. Additionally, the influence of stirring rates at 400 and 500 rpm for the HY-80 experiments was tested and found to have no significant effect. Therefore, a stirring rate of 400 rpm was maintained for all experiments.

At 2 h, the glycerol conversion was 65 % for the control experiment, whereas the glycerol conversion with zeolites varied from 67 % to 91 %, depending on the zeolites' framework type, pore morphology, and acidity. Interestingly, while most zeolites showed higher glycerol conversion than the control experiment at 2 h, HZSM5–23 and HY-5.1 resulted in similar or only slightly higher glycerol conversion, ranging from 67 % to 68 %. HZSM5–23 and HY-5.1 only performed better than the control experiment in terms of trivalerin yield, improving it from less than 1–2 %.

3.3.1. *Zeolite framework type and mesoporosity*

The differences in performance could arise from total acidity, hydrophilicity and hydrophobicity of the zeolite frameworks. While the framework is an intrinsic property of each zeolite type, total acidity, hydrophobicity and hydrophilicity are interrelated by the SiO_2/Al_2O_3 ratio. In this section, each property will be briefly examined and the effect of SiO_2/Al_2O_3 ratio will be discussed in more detail in Section 3.4.

Firstly, the effect of framework type can be compared. ZSM-5 zeolite is well known for having smaller pores compared to Y and BEA zeolites. Table 3 summarizes the characteristics of each zeolite type. The ZSM-5 zeolite framework (MFI type) consists of 10-membered rings, 3-dimensional channels with a size of 5.1–5.6 Å, and a maximum diffusible spherical diameter of 4.7 Å [58]. In contrast, the Y zeolite (FAU type) framework has the largest 12-membered rings with channel openings of 7.35 Å and supercage internal diameters of 11.24 Å, with a maximum diffusible diameter of 7.35 Å. The BEA framework results from the intergrowth of two distinct polymorphs A and B, consisting of a 12-membered ring structure with a maximum diffusible diameter of 5.94 Å for polymorph A and 5.88 Å for polymorph B [58]. According to the framework structures, the channel opening sizes rank from largest to smallest as follows: Y > BEA > ZSM-5. Therefore, HZSM5–23's poorer performance than all BEA catalysts may be attributed to its smaller channel opening. The effect of zeolite framework was highlighted in a study by Fernandes et al., in which various zeolite framework types—HMCM-22, HUSY, HBEA, HZSM-5 and HMOR—were investigated for levulinic acid conversion. The authors reported no clear correlation between the total acidity of the zeolites and their activity. Instead, the activity was related to their structural features, steric effects, and the formation of intermediates within the confined zeolite channels [59]. Nevertheless, despite having the largest framework channel opening (7.35 Å), HY-5.1 did not outperform any of the HZSM5 variants with SiO_2/Al_2O_3 ratios of 23, 30, and 80, which feature significantly smaller channel size. This indicates that framework size is not the determining factor in the esterification of glycerol and VA within the tested zeolite series.

Table 3
Zeolite framework type, channel opening size [58].

Framework Type	Largest member ring	Channel opening	Maximum diameter to be included	Maximum diffusible diameter
ZSM-5 (MFI)	10	5.1–5.6 Å	6.36 Å	4.7 Å
Y (FAU)	12	7.35 Å	11.24 Å	7.36 Å
BEA	12	5.5–7.7 Å	6.59–6.82 Å	5.88 – 5.94 Å

The results in Fig. 5 cannot be explained solely by looking at the framework type and channel openings. Although HY-5.1 has the largest framework channel opening, it performed worse than all HBEA and both HZSM5–30 and HZSM5–80. This means that it could be the acidity, mesoporosity or hydrophilicity of the zeolite or a combination thereof that is responsible for the activity. Although zeolites are generally microporous materials, they may contain mesoporosity obtained by their preparation methods as previously discussed in Section 3.2, like in the case of HY-80. Therefore, the N_2 physisorption results should be considered to examine the correlation between textural properties and catalytic activity. Glycerol conversions after 2 h were plotted against mesoporous surface area and mesoporous volume for all zeolites in Fig. 6a and Fig. 6b, respectively.

From Fig. 6a, a clear trend was observed for HY zeolites: as the mesoporous surface area increased, the glycerol conversion rose from 68 % to 84 %. A closer look at the N_2 physisorption isotherm of HY-5.1 (Fig. 2c) revealed a less prominent to absent hysteresis loop, indicating a predominantly microporous structure. This observation is consistent with the calculated microporous surface area (S_{micro}) and microporous volume (V_{micro}) values in Table 1. HY-5.1 indeed has the lowest mesoporous surface area among the tested zeolites, at only 42.4 m^2/g, compared to over 170 m^2/g for the others. The low mesoporosity of HY-5.1 likely restricts the diffusion of reactants and products to the active sites, which reduces the performance of microporous Y zeolite [60].

While HY zeolites exhibit a correlation between mesoporous area and activity, no clear trend is evident for HZSM-5, where the mesoporous area was similar (Fig. 6a). However, a relationship between mesoporous volume and glycerol conversion is observed across all three zeolite frameworks. Fig. 6b shows that glycerol conversion increases with rising mesoporous volume for HY, HBEA, and HZSM-5. The beneficial effect of mesoporosity is consistently observed throughout the experiments.

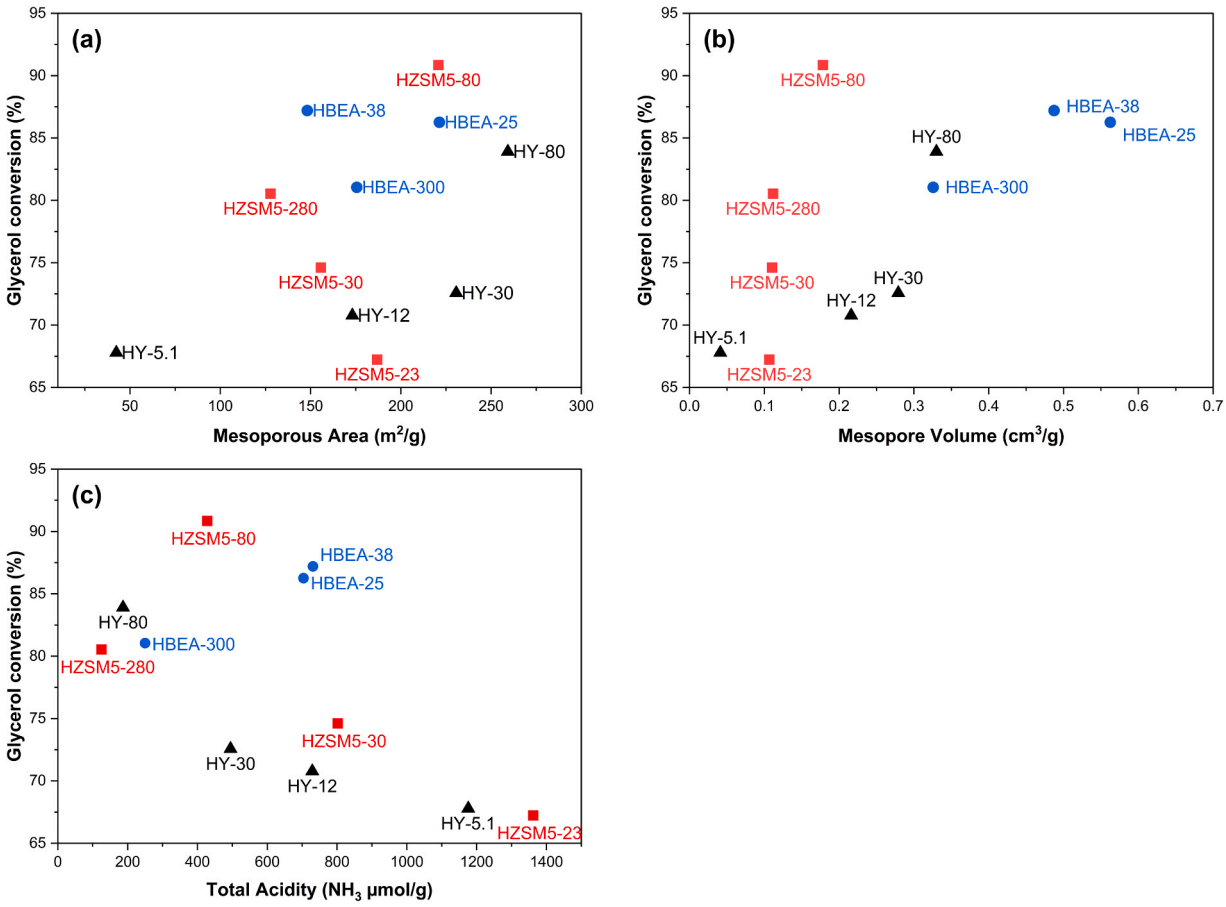

Fig. 6. Glycerol conversion after 2 h reaction time plotted against a) mesoporous area, b) mesopore volume, c) total acidity of the zeolites. Reaction conditions were 130 °C, 400 rpm stirring rate, 1 wt% catalyst loading, 5:1 acid-to-glycerol feed mole ratio with total reflux.

3.3.2. *Zeolite acidity*

Interestingly, total acidity appears to show no clear correlation with catalytic performance, as shown in Fig. 6c. Although HY-5.1 exhibits one of the highest acidities among the tested zeolites (1176 μmol NH_3/g, Table 1) and a B/L acid type ratio 1.62 (Table 2), its esterification reactivity remains low. This suggests that total acidity alone is not a reliable predictor of catalytic performance. Another notable observation is that HZSM5–23, despite having even higher acidity (1362 μmol NH_3/g), did not outperform HY80, which had significantly lower acidity (187 μmol NH_3/g). One possible explanation is the larger mesoporous surface area of HY-80 (259.3 versus 186.9 m^2/g). Additionally, the spent HZSM5–23 catalyst appeared more yellow-brown in color compared to spent HY-80 (Figure S3c) and spent HZSM5–80 (Figure S3b), indicating greater deactivation and accumulation of organic compounds. This deactivation may result from the high density of acid sites, particularly strong acid site, as evident from the prominent NH_3-TPD peak in the 350–450 °C range (Fig. 3a). Deactivation of ZSM-5 by coke deposition at strong acid sites is a well-known limitation in several gas phase reactions, such as methanol dehydration [61], methanol to olefin conversion [62], olefin oligomerization [63], and olefin production from dimethyl ether [64]. Guisnet [65] reviewed zeolite deactivation by coking in petrochemical refining and identified acid site strength and density, as well as microporosity, as key factors contributing to rapid coke formation. Brønsted acid sites are active in isomerization, oligomerization, and condensation reactions, which can lead to the formation of carbonaceous compounds that become trapped in micropores, hindering reactant diffusion. HY-5.1 also showed slightly more yellow color compared to HY-80 (Figure S3a). The inferior performance of HY-5.1 and HZSM5–23 may thus be attributed to their high total acidity combined with small pore size and limited mesoporosity. This mechanism may also explain the inconsistent performance observed across the HZSM-5 series in Fig. 6, where mesoporosity ranged from 127.8 to 220.8 m^2/g. Although HZSM5–23 and HZSM5–30 had similar mesoporosity to HZSM5–80, their significantly higher acidity (Table 1) may have led to faster deactivation and reduced esterification activity.

Among the zeolites with a similar total acidity of 700–800 μmol NH_3/g (HBEA-25, HBEA-38, HZSM5–30, and HY-12), HBEA-25 and HBEA-38 showed superior glycerol conversion and DV and TV selectivity. The glycerol conversion for HBEA-38 reached 87.2 % at 2 h, compared to 74.4 % and 75.3 % for HZSM5–30 and HY-12 respectively (Fig. 5). The yields for DV and TV were also the highest for HBEA-38. Although HY-12 possesses the largest cavity size among the three framework types, it did not demonstrate greater reactivity than HZSM-30 with a much smaller framework channel opening size. This is rather unexpected as the larger channel opening of the zeolite framework should lead to less diffusion resistance. One of the possible reasons for the inferior performance of HY-12 is its highly hydrophilic nature due to its low SiO_2/Al_2O_3 ratio. Indeed, HY-12 has a much lower SiO_2/Al_2O_3 compared to HBEA-38 and HZSM5–30 (see Table 1). This finding emphasizes the importance of the interplay between the catalysts' acidity, hydrophilicity/hydrophobicity, and pore morphology. The effect of the SiO_2/Al_2O_3 ratio, acidity, and catalysts' hydrophobicity will be discussed in more detail later.

When comparing all tested zeolites at various SiO_2/Al_2O_3 ratios, HZSM5–80, HBEA-38, and HY-80 were evaluated as the best among their zeolite types due to their high glycerol conversion and higher DV and TV ester yields. These three zeolites exhibit mesoporosity characteristics, as seen in the N_2 physisorption isotherms (Fig. 2). HZSM5–80

exhibited the highest glycerol conversion at 91 % and 44 % total DV and TV product yields respectively at 2 h reaction time, while the control only resulted in 14.5 % yield of DV and less than 1 % yield of TV (Fig. 5). However, the highest amount of side products after 6 h (3.9 % of total FID area) was also found in the HZSM5–80 product mixture and HBEA-38 resulted in a similar amount (3.2 % FID area side products, see Table S1). On the other hand, only 0.3 % FID area side products were detected in the HY-80 product mixture by GC-MS/FID. Therefore, despite having somewhat lower glycerol conversion and di, and tri-ester yields, HY-80 was selected as the best-performing catalyst and further examined for process parameter optimization in Section 3.6.

3.4. Effect of SiO_2/Al_2O_3 ratio and hydrophilicity/hydrophobicity

To better understand the role of a zeolite's properties in esterification reactivity, the glycerol conversion with zeolites at varying SiO_2/Al_2O_3 ratios was plotted against reaction time (2–6 h) in Fig. 7 for comparison. Generally, higher glycerol conversion was observed with a higher SiO_2/Al_2O_3 ratio for both HZSM-5 and HY zeolites. The SiO_2/Al_2O_3 ratio is an important parameter for zeolite catalysts as it influences their hydrophilicity, hydrophobicity, and acidity. A higher amount of Al in the zeolite frameworks (lower SiO_2/Al_2O_3 ratio) results in a higher density of Brønsted acid sites, which results in higher hydrophilicity due to absorption of water [66] or polar molecules, which could be on the framework Si-OH-Al bridging hydroxyl group or nest silanol Si-OH-Si groups. Brønsted acid sites in low SiO_2/Al_2O_3 zeolites can be deactivated by water or adsorption of polar organic molecules, leading to lower esterification reactivity. This possible effect of hydrophilicity at low SiO_2/Al_2O_3 ratio combined with lower mesoporosity, is evident for the HY-5.1 which have SiO_2/Al_2O_3 ratios of 5.6. HY-5.1 samples exhibited the lowest glycerol conversions among the tested zeolites, reaching only 67 % conversion after 2 h (Fig. 5). Despite its high acidity (1167.5 μmol NH_3/g), HY-5.1 did not outperform less acidic zeolites, possibly due to its strong hydrophilic nature or the deactivation from strong acid sites as discussed in Section 3.3. Our findings for the Y-series zeolites agree with those reported by Osatiashtiani et al. [67], who investigated the esterification of bio-oil using Y zeolites. The authors reported that the surface polarity of Y zeolite, measured via inverse gas chromatography, decreased with increasing Si content. Furthermore, the esterification activity improved with greater hydrophobicity and acid strength [67].

While HZSM-5 and HY zeolites generally show better catalytic performance in esterification with a higher SiO_2/Al_2O_3 ratio, the SiO_2/Al_2O_3 ratio of HBEA zeolites appeared to have a weaker impact on the catalytic performance in terms of glycerol conversion (see Fig. 7b). Interestingly, HBEA-25 with the lowest SiO_2/Al_2O_3 ratio of 12.9, performed similarly to HBEA-38 and HBEA-300. Similarly, BEA zeolites with a wide range of SiO_2/Al_2O_3 (13, 20, 220), employed for esterification of o-cresol and acetic acids produced almost identical yields of cresol acetate [37].

However, acidity is important which can explain why HZSM5–280 exhibited lower activity compared to HZSM5–80. The best SiO_2/Al_2O_3 ratio for both HZSM-5 and HY zeolites, of those examined, was found to be at 87–89, where the glycerol conversion could reach 90 % within 4 h.

Since the esterification of VA and glycerol proceeds through a series reaction, product distribution is expected to correlate with glycerol conversion — higher conversion (occurring after longer time) typically favoring the yield of the higher esters DV and TV. However, because glycerol is the limiting reagent, high glycerol conversion may not directly translate to proportional consumption of VA or consistent product distribution. Therefore, the effect on product yield is specifically examined in Fig. 8. After 4 h, the zeolites resulted in similar glycerol conversion, ranging from 80 % to 90 %, allowing for a comparison of how the inherent properties of the zeolites may influence product distributions. Within this narrow range of glycerol conversion, there were significant differences in ester product distribution, highlighting the impact of the SiO_2/Al_2O_3 ratio and zeolite framework. Zeolites, with a low SiO_2/Al_2O_3 ratio generally produced lower DV and TV yields compared to those with higher SiO_2/Al_2O_3 ratios. Specifically, HY-5.1 exhibited DV and TV yields that were 18–20 % lower than those of zeolites with a higher performing SiO_2/Al_2O_3 ratio of 87–88.6.

This finding regarding the effect of the SiO_2/Al_2O_3 ratio highlights the importance of the hydrophilic or hydrophobic nature of the zeolites in esterification. In esterification reactions, where water is inevitably formed as a by-product, hydrophobic catalysts are preferred due to their greater resistance to active site blockage by water molecules [33,52]. The hydrophobic nature of zeolites also facilitates the diffusion of hydrophilic reactants such as VA and glycerol and the release of ester products from the active site [52]. Our results agree with previous literature by Prinsen et al. [52] and Fawaz et al. [33]. Similar to our result in Fig. 3c where total acidity did not show clear effect on the glycerol conversion, Prinsen et al. [52] reported that the reactivity of palmitic acid esterification with methanol did not show a strong dependence on the total acidity of zeolites but rather exhibited a strong correlation with the hydrophilic nature and porosity of the zeolites. The authors investigated HZSM-5 and HY zeolites and reported that HY with a SiO_2/Al_2O_3 of 60, possessing higher hydrophobicity than HY with a SiO_2/Al_2O_3 of 5.2, converted 100 % of palmitic acid after 3 h at 70 °C, whereas HY-5.2 performed worse, giving approximately 20 % glycerol conversion under the same reaction conditions [52]. Similarly, Fawaz et al. studied the esterification of linoleic acid using HZSM-5 at varying SiO_2/Al_2O_3 ratios. The authors found that HZSM-5 with a SiO_2/Al_2O_3

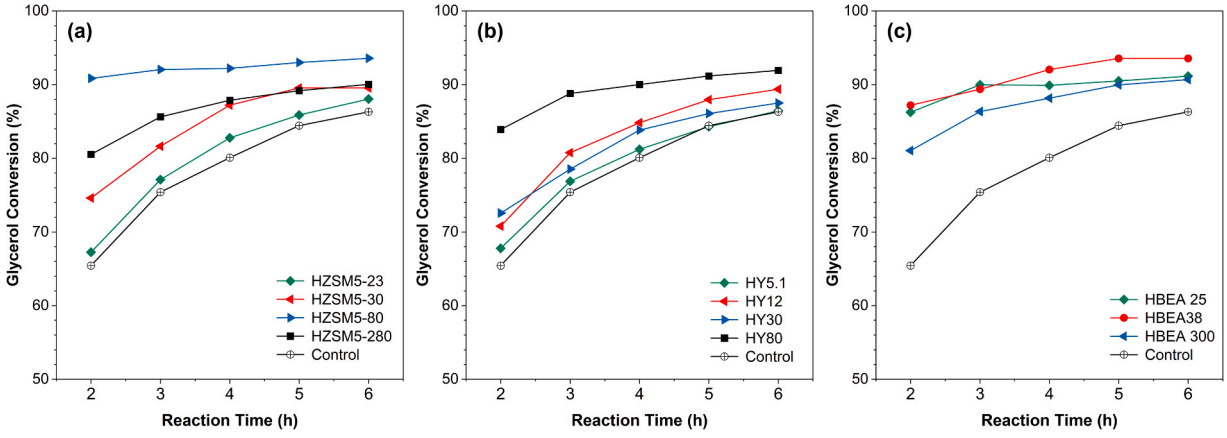

Fig. 7. The conversion of glycerol of (a) ZSM-5, (b) Y and (c) BEA zeolites as a function of reaction time at 130 °C, 400 rpm, 5:1 acid-to-glycerol mole ratio, 1 wt% catalyst loading and under total reflux.

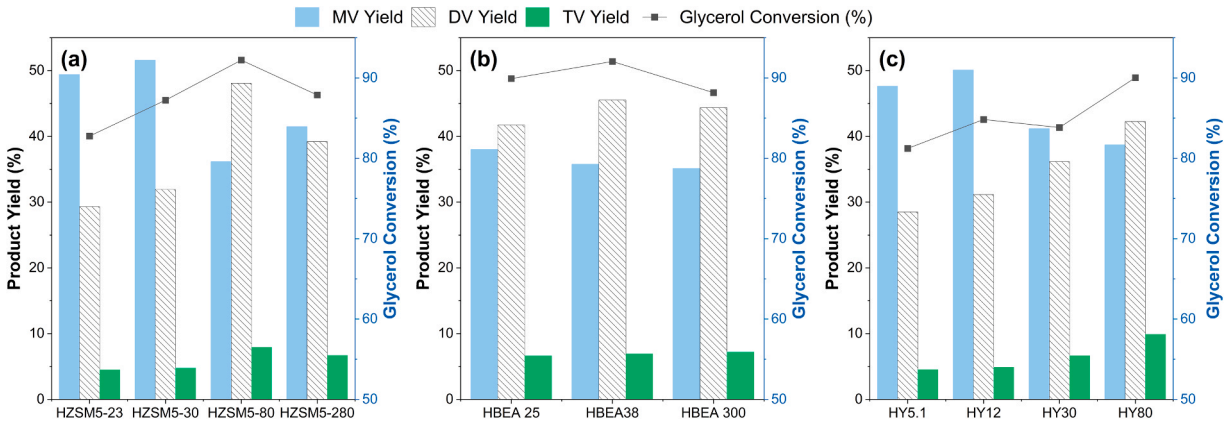

Fig. 8. Comparison between a) HZSM-5, b) HY, and c) HBEA at different SiO_2/Al_2O_3 ratios at 4 h, 130 °C, 400 rpm, 5:1 acid-to-glycerol mole ratio, 1 wt% catalyst loading under total reflux.

ratio of 106 gave the highest methyl linoleate yield of 79.8 % compared to HZSM-5 with SiO_2/Al_2O_3 ratios of 28.8 and 66.6. During the initial reaction stages, low SiO_2/Al_2O_3 ratio HZSM5 had higher reactivity but was overtaken by high SiO_2/Al_2O_3 ratio HZSM5 after 4 h due to its hydrophobic nature [33].

3.5. Effect of pore morphology and mesoporosity

As discussed in Section 3.3.1, mesoporosity appeared to be a more influential factor the zeolite framework type. This section revisits the role of mesoporosity and expands the discussion by comparing the two best-performing zeolites HY-80 and HZSM5–80, which have similar SiO_2/Al_2O_3 ratios. Both catalysts exhibited high catalytic performance in terms of both glycerol conversion and product selectivity in a similar manner. Fig. 8 shows that HY-80 and HZSM5–80 converted more than 90 % of glycerol and produced total yields of DV and TV at 52 % and 56 %, respectively after 4 h. Although the samples exhibited similar SiO_2/Al_2O_3 ratios of 87–88.6, the acidity was very different, where the total acidity was 428 μmol NH_3/g for HZSM5–80 whereas 187 μmol NH_3/g for HY-80 (see Table 1). Even though HY-80 has lower acidity, its performance remains comparable to HZSM-80. Further analysis of the N_2 physisorption results reveals that BET surface area for HZSM5–80 is 479.5 m^2/g, while HY-80 has a considerably larger surface area of 808.1 m^2/g. As discussed in Section 3.1 that the N_2 physisorption isotherms for HY-80 and HZSM5–80 both reveal presence of mesoporous structures. However, HY-80 possesses a higher mesopore surface and volume (see Table 1), which could contribute to reduced diffusion limitations and enhanced active site accessibility compared to HZSM5–80. This finding reemphasizes yet another crucial factor: the pore morphology of the catalysts.

It is evident from comparing the HZSM5–80 and HY-80 results that the catalyst's mesoporosity is a critical factor in the esterification of VA and glycerol, in addition to zeolite hydrophobicity and acidity. The higher total surface area and mesopore surface area of HY-80 may contribute to its comparable esterification reactivity, despite having lower total acidity. Similarly, a study by Gomes et al. revealed that introducing mesoporosity into MOR zeolite through desilication increased the conversion of oleic acid to methyl oleate from 44 % to 70 % [39]. The author attributed the inferior performance of the parent MOR zeolites to its lack of a three-dimensional framework or super-cavities, which restrict the mobility of bulky intermediates within the zeolite pores. In contrast, the desilicated MOR exhibited a hierarchical pore structure, likely enhancing reagent accessibility and facilitating the formation of a stabilized intermediate within the pore [39]. In addition to improving diffusion pathways within the catalyst crystal, dealumination and desilication processes create structural defects that form nested hydroxyl groups (silanol nests). These groups can interact via hydrogen bonding due to the absence of Si and Al atoms, further enhancing the catalytic reactivity [60].

Our findings also align with the previous study done by Zhang et al. [36], where HY-5.1, HY-30, and HY60 (CBV300, CBV720, CBV760 from Zeolyst) were investigated for the esterification of methanol and propionic, hexanoic, and lauric acids. They found that the conversion of carboxylic acid over different HY zeolites correlates with the kinetic diameter of the acids, suggesting that the steric hindrance of the reaction inside the porous zeolites is significant. Despite the substantial reduction of acid sites compared to microporous HY-5.1, HY-30 and HY-30 showed superior esterification activity for longer chain acids like hexanoic and lauric acids. The authors characterized the mesoporosity of the three zeolites extensively, concluding that the presence of large mesopores (>5 nm) in HY-30 and HY60 is the crucial factor in the liquid phase esterification for bulky compounds [36].

To summarize, overall higher glycerol conversion and formation of higher esters DV and TV products was observed with a higher SiO_2/Al_2O_3 ratio. This can be linked both to increased hydrophobicity as well as the increased mesoporosity seen for many of the samples when increasing the SAR (especially for zeolite Y) as discussed in relation to Fig. 6. However, it must be noted that in this study it was not possible to distinguish the individual effects of hydrophobicity and mesoporosity. High-silica zeolites, with a high SiO_2/Al_2O_3 ratio, are more hydrophobic and tend to contain more mesoporosity compared to their high-alumina counterparts. Additionally, they possess a lower density of strong Brønsted acid sites, which could help to reduce the formation of side products and coke, thereby mitigating catalyst deactivation. The improved performance observed may therefore result from a combination of factors: appropriate pore morphology, a balanced distribution of acid strength and site density, and enhanced hydrophobicity.

3.6. Influence of reaction parameters with HY-80

Based on the zeolite screening results in Sections 3.3–3.5, HY-80 was selected for further process parameter optimization due to its combination of relatively high activity and low yield of side products. The reduced formation of side products also implies less catalyst deactivation during continuous use, offering an industrial advantage over HZSM5–80 and BEA-38. The influences of reaction parameters such as acid-to-glycerol feed ratio, temperature, and catalyst loading were studied using HY-80.

Three different VA to glycerol feed mole ratios (3:1, 5:1, and 3:2) were examined using HY-80 zeolite at 130 °C, 400 rpm, 1 wt% catalyst loading, and total reflux reaction conditions. The addition of excess VA significantly improved glycerol conversion, as shown by results from the 5:1 feed mole ratio in Fig. 9a. Moreover, Fig. 9c and Fig. 9d illustrate that an excess VA led to consistently higher yields of DV and TV

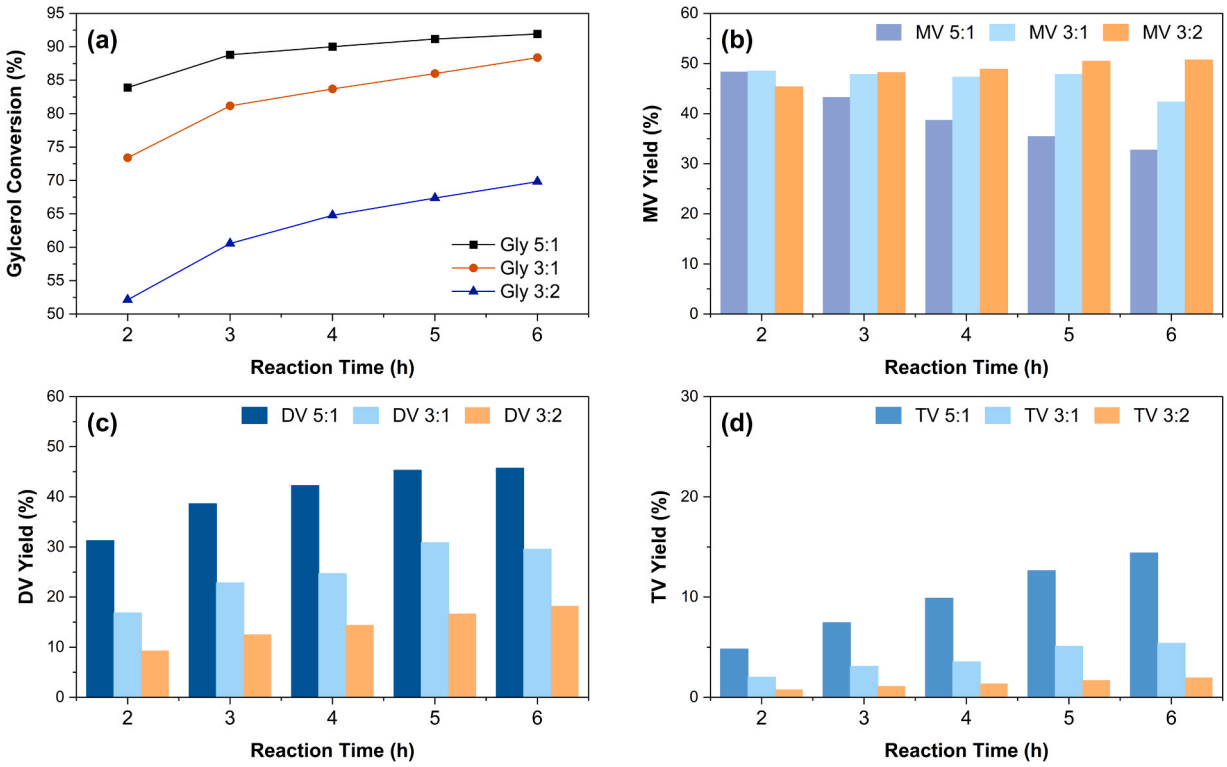

Fig. 9. Using HY-80, the effect of valeric acid: glycerol feed mole ratio (5.1, 3:1 and 3:2) on a) glycerol conversion b) MV yield c) DV yield and d) TV yield at 130 °C, 400 rpm, 1 wt% catalyst loading under total reflux.

throughout the 6 h reaction period. This improvement is expected given excess availability of VA to react with MV, thereby increasing production of DV and TV. Excess VA may also improve mixture miscibility by decreasing mixture viscosity, as glycerol is a highly viscous substance. The excess VA can act as a solvent, distributing and improving miscibility of glycerol, VA and the zeolite catalyst. On the other hand, an increase in glycerol mole ratio to 3:2 resulted in a lower yield of DV and TV, with the majority of product formed being MV at a consistent 40–50 % yield throughout the 6 h reaction time (Fig. 9a). To achieve a higher yield of DV and TV, an excess of VA is required to further drive the higher ester formation rate. These results are consistent with the work by Kirumakki et al. [68], who found that excess alcohol reduced the esterification rate of acetic acid and benzyl alcohol over zeolites. This suggests possible competitive adsorption between alcohol and carboxylic acid on the active sites. The presence of excess alcohol species led to a decreased rate, indicating that the adsorption of carboxylic acid on the zeolite surface is a crucial step in esterification. [68].

Next, the effect of reaction temperature is shown in Fig. 10 at three different reaction temperatures: 95 °C, 110 °C, and 130 °C using HY-80 zeolite. The glycerol conversions were plotted and compared with a control experiment without catalyst at corresponding temperatures in Fig. 10a. The data in Fig. 10 reveals a clear correlation between elevated temperature and enhanced glycerol conversion and higher esters product formation. Glycerol conversion improved from 24 % to 65 % when the reaction temperature increased from 95 °C to 130 °C in the control experiment at 2 h reaction time. Due to low glycerol conversion, the majority of ester products were MV, with no TV formed at 95 °C during the 6 h control experiment (see Figure S4). The presence of HY-80

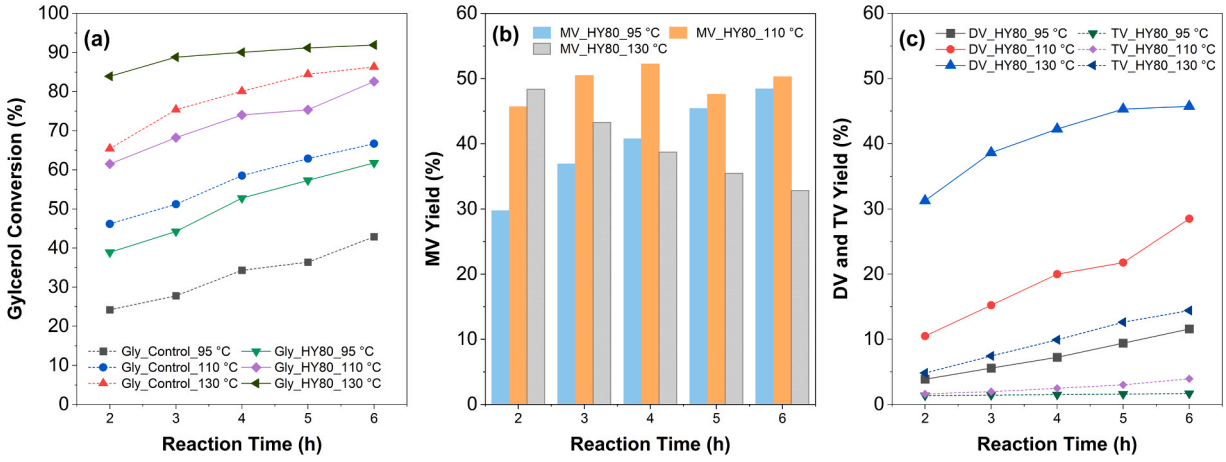

Fig. 10. Glycerol conversion and product yields at different reaction temperatures a) glycerol conversion with HY-80 and control experiment (without catalyst), b) MV yield with HY-80, C) DV and TV yield with HY-80, at 400 rpm, 5:1 acid-to-glycerol feed mole ratio, 1 wt% catalyst loading under total reflux.

improved glycerol conversion by 15 % and 22 % at 95 °C and 110 °C, respectively. Another effect of elevated temperature is higher miscibility between glycerol and VA due to lower glycerol viscosity at elevated temperatures [69], which can facilitate the nucleophilic attack of the oxygen atom of the glycerol molecule on the protonated carbonyl in VA. When looking at MV yield, HY-80 at 95 °C produced comparable yields as 110 °C after 6 h reaction time (Fig. 10b), whereas the DV yields at 95 °C were significantly lower due to low glycerol conversion (Fig. 10c). During the first 3 h at 110°C, the TV yield was less than 3.5 %, while at 130°C, a 6 % TV yield was achieved within just 2 h.

Increased temperature accelerates the reaction, leading to higher glycerol conversion, with higher DV and TV yields. However, it is also important to explore whether temperature inherently influences product selectivity by comparing the product distributions at different temperatures but with the same glycerol conversion. From Fig. 10a, comparing the results at 95 °C and 110 °C, at 6 h and 2 h respectively, the glycerol conversions are 63 % and 68 %. Under these conditions with similar glycerol conversions, the yields of MV, DV and TV are close: 41–48 % for MV, 10–11 % for DV and 1.6–1.7 % for TV (Fig. 10b and Fig. 10c). These results indicate that temperature does not inherently control product selectivity, suggesting little difference in the activation energies of the three esterification reactions.

Finally, five different catalyst loadings ranging from 0.5 to 4 wt% were tested for esterification reactivity under reaction conditions of 130 °C, 5:1 acid-to-glycerol feed mole ratio and 400 rpm using HY-80 (Fig. 11). The data presented in Fig. 11 shows that the conversion of glycerol is increasing with catalyst loading, as well as the selectivity to DV and TV. These results are expected since higher catalyst loading provides a higher number of Brønsted acid sites that can catalyze the esterification reaction. Notably, catalyst loadings of 3 and 4 wt% were able to achieve 89 % glycerol conversion after 1 h reaction time at 130 °C, reaching glycerol conversion equilibrium after 3 h (Fig. 11a). The best reaction condition, of those examined in this work is: 130 °C, 5:1 acid to glycerol feed mole ratio, 400 rpm stirring rate and 4 wt% catalyst loading.

3.7. HY-80 catalyst reusability and stability

The reusability of the HY-80 catalyst was assessed by performing four successive 3 h batch-wise esterifications of fresh VA and glycerol feeds at 1 wt% catalyst loading, 130 °C, 5:1 acid-to-glycerol feed mole ratio. At the end of each reaction cycle, HY-80 was separated from the reaction mixture via centrifugation, weighed, and used directly with fresh feed in the next cycle without any regeneration treatment. After each cycle, a small fraction of HY-80 may be lost during collection and centrifugation due to its fine powder nature. Approximately 0.04–0.06 g of fresh, dried HY-80 was added to compensate for catalyst mass loss before each subsequent cycle (see supplementary information for detailed description).

Fig. 12 shows a slight drop in glycerol reactivity after four cycles, with about a 2 % decrease in glycerol conversion. The total yield of DV and TV decreased somewhat from 44 % to 39 % after the four cycles, with a corresponding increase in the yield of MV from 43.8 % to 48.4 %. Similar results of HY and HZSM-5 zeolites' superior recyclability were reported by several studies with longer acid chains, such as oleic acid [34] and linoleic acid [33,52].

It should be noted that catalysts recovered after each reaction cycle became slightly yellow (see Figure S5), indicating the presence of some residual of organic compounds or side products absorbed on the spent catalyst formed during the esterification experiment. The catalyst recovered after the fourth reaction cycle was washed with ethanol three times and dried at room temperature. However, the yellow color remained, suggesting the adsorbed species were not ethanol-soluble. To quantify the insoluble material, the washed sample was analyzed with TGA, which revealed a 15 wt% mass loss (see Figure S6). This accumulation of organic molecules likely blocks active sites and causes to a decline in catalytic performance. However, it should be considered that the ethanol adsorption within the zeolite pore may contribute to the

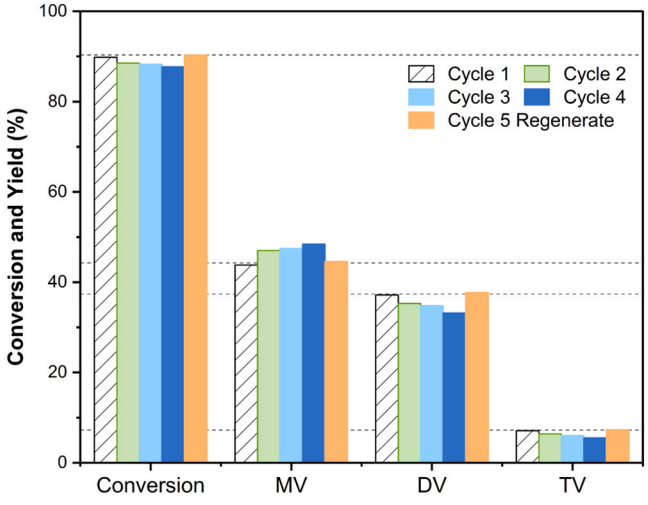

Fig. 12. Glycerol conversion, ester product yields after HY-80 reuse in VA and glycerol esterification reaction cycles at 130 °C, 5:1 acid-to-glycerol mole ratio, 1 wt% catalyst loading, 400 rpm under total reflux. Prior to cycle 5, the catalyst recovered from cycle 4 underwent a regeneration treatment by re-calcination.

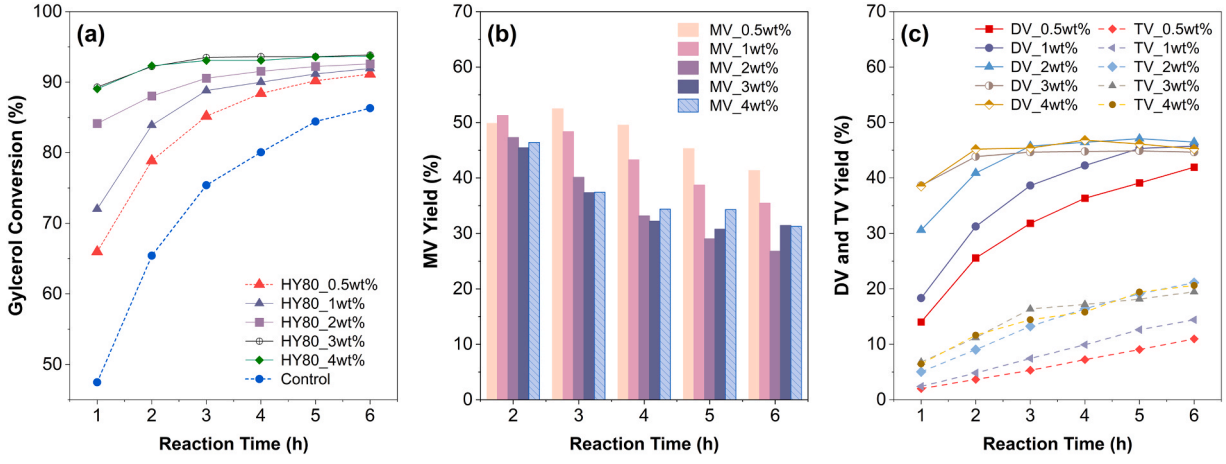

Fig. 11. HY-80 loading influence on a) glycerol conversion, b) MV yield, c) DV and TV yield, at 130 °C, 5:1 acid to glycerol mole ratio, 400 rpm under total reflux.

mass loss. Xu et al. conducted ethanol TPD experiments on BEA catalysts and observed the release of ethene and water between 200 and 300 °C [70], indicating that part of the mass loss may be attributed to ethanol desorption. Finally, the washed and dried spent catalysts, recovered from cycle 4, were regenerated by calcination at 500 °C for 6 h, following heating at a rate of 5 °C/min. After this regeneration treatment, the color of the catalyst became white again, suggesting removal of the organic species. The catalytic performance of this regenerated catalyst was examined in a fifth reaction cycle, as shown in Fig. 12. The regenerated HY-80 exhibited the same catalytic performance as in reaction cycle one, indicating that the regeneration treatment fully restored the catalytic activity. Further analysis by N_2 physisorption revealed an increase in surface area from 808.1 m^2/g for fresh HY-80–858.6 m^2/g for regenerated HY-80 and a slight increase in pore volume (0.63 cm^3/g) compared to 0.59 cm^3/g the fresh HY-80. The isotherm in Figure S7 showed a hysteresis type H4, similar to the fresh HY-80 catalyst. The crystalline structure after regeneration was investigated by XRD of the spent catalyst shown in Figure S8, compared to that of the fresh catalyst. The XRD data shows no clear reduction in crystallinity after four cycles of esterification and the subsequent high-temperature regeneration treatment. The regenerated HY-80 was also analyzed for Si and Al content by the ICP-SFMS method and found to be 82, having no significant change in SiO_2/Al_2O_3 ratio after four cycles of esterification and regeneration treatment. SEM images of fresh and spent catalysts show no significant deviation in catalyst morphology (Figure S9). From the characterization results of the regenerated catalyst, it is clear that the catalyst structure maintains its crystallinity and integrity after four reaction cycles, supporting that zeolites are highly stable catalysts for esterification reactions. The HY-80 zeolite showed potential for continuous esterification application and the possibility for regeneration via calcination due to its highly stable framework structure and acid sites. Furthermore, due to the reaction mixture being acidic (pH=3–4), a few experimental liquid product mixtures were selected and tested for any leached Al and Si species by ICP-SFMS measurement. The Si and Al content in all liquid samples was found to be below the detection limit (Table S2).

In addition to direct catalyst reuse, a mild regeneration method involving solvent washing was investigated. This procedure consisted of two ethanol washes followed by a single acetone wash to dissolve reactants or organic compounds adsorbed on the catalyst surface. After drying, the catalyst was weighed to the desired amount and reused in the experiment without further treatment (Scheme S1). The results are shown in Figure S10 in the supplementary information. Figure S10 shows that solvent washing resulted in a slight improvement in catalyst performance from cycle 1–3, compared to the untreated catalyst shown in Fig. 12. Glycerol conversion remained relatively stable, with a modest increase in MV yield and a slight decrease in TV. However, in cycle 4, glycerol conversion dropped by 3 %, accompanied by a 4 % increase in MV and a 5 % decrease in DV. At this stage, the performance of the washed and unwashed catalysts was comparable, possibly stemming from the accumulation of insoluble products within the catalyst pores or on its surface.

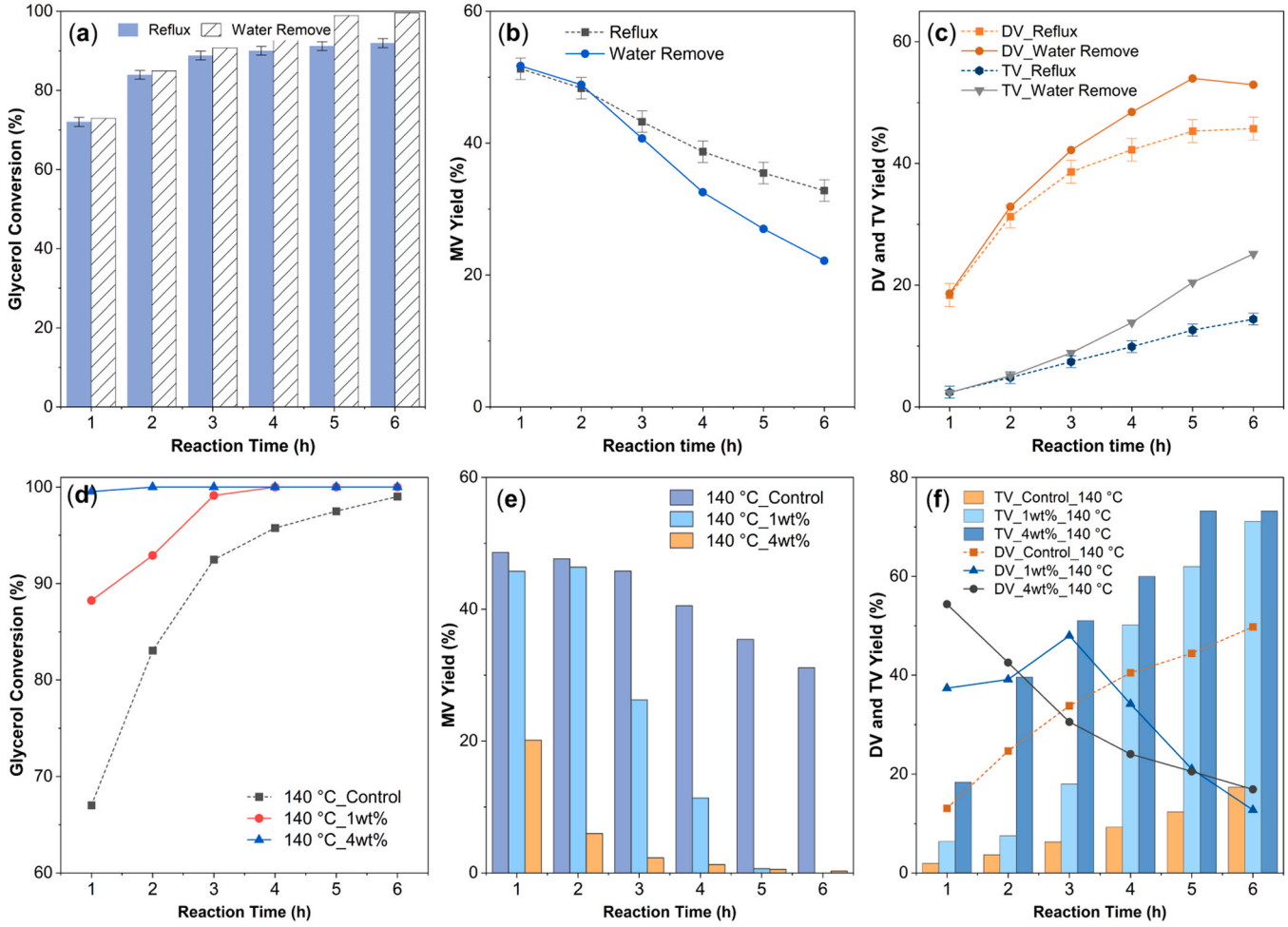

Fig. 13. Continuous water removal esterification at 5:1 acid-to-glycerol mole ratio, 400 rpm using (a) - (c) Comparison of water removal and total reflux results with 1 wt% catalyst loading, 130 °C, (d) - (f) Effect of catalyst loading with water removal at 140 °C and catalyst loading 0–4 wt%.

3.8. Continuous water removal esterification

To explore the potential for carrying out the esterification by a catalytic distillation process with HY-80, the reaction was conducted with a continuous water removal reactor setup under reaction conditions of 130 °C, 5:1 acid-to-glycerol mole ratio, 400 rpm stirring and 1 wt% catalyst loading. Instead of the total reflux flask setup described in Section 3.3, a condenser was connected to one of the side flask necks and positioned downward. A round-bottom flask was connected to the end of the condenser to collect condensate. The results are compared against the total reflux conditions in Fig. 13a-c to illustrate the effect of continuous water removal. With water removal during the reaction, the glycerol conversion was not significantly improved during the first 3 h. However, during the 3–6 h reaction period, the equilibrium was pushed toward products as the glycerol was completely converted after 6 h at 130 °C, and a 5:1 acid-to-glycerol feed mole ratio. The maximum yield of DV obtained was 50 %, and TV yield significantly improved from 14 % to 25 % after 6 h. Note that with this setup, a minor amount of VA was lost due to evaporation, as the condensate collected contained 15–20 wt % VA, depending on the reaction conditions. This corresponds to a maximum loss of about 1.6 wt% of the total initial VA reactant mass.

To further increase the DV and TV yield, the reaction temperature was increased to 140 °C, and catalyst loading varied from 0 wt% to 4 wt % using HY-80 and a continuous water removal setup. It was found that 4 wt% HY-80 significantly enhanced the rate of glycerol conversion, achieving 99 % glycerol conversion within the first hour of reaction as shown in Fig. 13d. At elevated temperatures, the difference between the uncatalyzed (control) and zeolite catalyzed performance became even more observable. After 2 h, while both 1 wt% and 4 wt% catalyst loadings converted 92–100 % of glycerol, the control experiment resulted in about 84 % glycerol conversion with low DV and TV yields. Almost all MV was converted into DV and TV after 5 h in the HY-80 catalyzed experiment (Fig. 13b). The highest TV yield obtained was 73 % after 6 h of reaction time with complete glycerol conversion and less than 1 % MV yield present in the reaction mixture using 4 wt% catalyst loading. However, a considerable amount of heavy side products was detected in the GC-MS/FID chromatogram eluting after DV and TV. A summation of the multiple small FID side product peaks gave an area percentage totaling 12.3 % as reported in Table S3. A carbon balance based on the calibrated products formed and the feed reactants, indicated that 3.5 wt% of carbon was unaccounted and could thus represent the side-product yield, although with experimental error. The side products were not identified in this study. The complete chromatogram is shown in Figure S11 and the MS fragmentation of side products is shown in Figure S12 in the supplementary information. The GC analysis of the reaction mixture from the control experiment at the same reaction conditions did not show peaks of heavy side products. The spent catalyst color also turned browner (Figure S13) compared to the spent catalyst from the lower temperature (130 °C) standard esterification reaction under total reflux conditions (Figure S5).

Our results show promising stability and high yields of higher glycerol valerates (DV and TV) at a relatively low temperature (140 °C), under operating conditions that allow in situ water removal. Prior work by Kaur et al. involving glycerol and valeric acids [7,40], or butanoic acid [6] investigated sulfated iron oxide (SO_4^{2-}/Fe_2O_3) as the main catalyst. The authors reported a maximum TV selectivity of 74.9 % at 180 °C (Table 4) under reflux condition, along with 24.6 % selectivity to n-amyl isovalerate as a side product [40]. Note that the reaction conditions differ between this work and literature, particularly in terms of reactant mole ratios, reaction temperature and catalyst loading (see Table 4). Although this work did not explore reaction temperatures as high as those previously reported, HY-80 achieved 71 % TV and 12.7 % DV selectivity with complete glycerol conversion at 140 °C, under continuous water removal.

In contrast, under total reflux conditions (i.e., without water removal), HY-80 did not reach the TV selectivity of SO_4^{2-}/Fe_2O_3 (Table 4). This discrepancy is likely attributable to the much higher catalyst acid density (14.4 mmol H^+ g^{-1} [6]), increased catalyst loading, and elevated reaction temperature used in the latter study.

Notably, the SO_4^{2-}/Fe_2O_3 catalyst suffers from deactivation, exhibiting ~20 % lower acid conversion after three cycles in the esterification of butanoic acid and glycerol [6]. However, improved stability was observed under reactive distillation conditions with glycerol and valeric acid [7]. In contrast, the zeolite catalysts used in this study can be readily regenerated by calcination without loss of framework integrity, underscoring their operational robustness and industrial appeal for tailoring DV/TV distributions.

4. Conclusions

This study evaluated solid acidic zeolites as potential heterogeneous acid catalysts in the esterification of glycerol and valeric acid, to produce green esters. Three types of zeolites in their protonated forms, including BEA, ZSM-5, and Y-zeolite, were tested at varying SiO_2/Al_2O_3 ratios for their catalytic activity. Zeolites with appropriate SiO_2/Al_2O_3 ratios, mesoporosity, and acidity achieved over 90 % glycerol conversion after 3 h of reaction time, with over 95 % yield of ester products and with over 60 % selectivity toward the higher di- and tri-ester products (DV and TV).

The zeolite screening tests conducted across varying SiO_2/Al_2O_3 ratios highlighted the critical roles of active site accessibility, acidity, and catalyst hydrophobicity on performance. Among the tested zeolite types, HZSM-5, HY, and HBEA−SiO_2/Al_2O_3 ratios of 87, 88.6 and 45, respectively, −exhibited the best performance within their respective framework types. This enhanced activity can be attributed to their mesoporosity and relatively high SiO_2/Al_2O_3 ratios, which could have provided adequate hydrophobicity to tolerate water formed during the esterification reaction. Highly acidic zeolites with low SiO_2/Al_2O_3 ratios and high microporosity, such as HY-5.1, performed poorly, possibly due to their hydrophilic nature and limited diffusion of reactants and products. However, zeolites with high SiO_2/Al_2O_3 ratios, containing a larger majority of stronger more active Brønsted acid sites, as well as

Table 4
Comparison of valeric acid and glycerol esterification activity for reported catalyst systems.

Catalyst	Temperature (°C)	Glycerol to Acid mole ratio	Catalyst Loading	Time	Conversion	Ester Selectivity (%)	Ref.
Sulfated Iron oxide	142.5	1:3	13 g/L	6 h	62.5 % Acid conversion	71.9 % TV 2.1 % DV 24.58 % n-amyl isovalerate	[40]
Sulfated Iron oxide	180	1:3	13 g/L	6 h	69.5 % Acid conversion	74.9 % TV 1.6 % DV 23 % n-amyl isovalerate	[40]
HY-80 zeolite	130	1:3	~10 g/L (1 wt %)	6 h	88.4 % Glycerol conversion	5.1 % TV 27.0 % DV 39.2 % MV	This work
HY-80 zeolite	140, Water Removal	1:5	~10 g/L (1 wt%)	6 h	100 % Glycerol conversion	73 % TV 16.9 % DV	This work

higher mesoporosity were highly beneficial for esterifying glycerol and VA. This structure facilitates the access of reactant molecules to the active Brønsted acid sites inside the zeolite framework. No clear correlation was observed between zeolite framework channel size and esterification activity due to the complex interplay among acidity, mesoporosity and hydrophilicity of the zeolites studied. For example, HZSM5–80 outperformed HY-5.1, despite having a smaller channel opening, which can be attributed to the presence of mesoporosity in HZSM5–80, whereas the HY-5.1 sample exhibited low microporosity.

HY-80 was chosen for further optimization of process parameters because it exhibited both relatively high activity and minimal formation of side products. The effect of reaction temperature on DV and TV formation was significant, with temperatures above 110 °C required for a 6 h reaction time to produce the highest tri-ester product (TV). However, there appears to be little difference in the activation energies of the esterification reactions, so temperature had no remarkable inherent effect on product selectivity. Furthermore, under the best reaction conditions under total reflux operation – using a 5:1 acid-to-alcohol mole ratio, 130 °C, and 4 wt% HY-zeolite loading (SiO_2/Al_2O_3 of 88.6) – a maximum total yield of 65 % for higher substituted di- and tri-esters (DV and TV) was obtained after 6 h of reaction time. When the reaction was conducted at 140 °C, using the same feed ratio and catalyst loading, but with continuous water removal, TV yield increased to 73 % and the combined yield of DV and TV rose to 90 %, with less than 1 % MV yield. However, at this high temperature the by-product formation was significant.

Finally, recycling tests with Y-zeolite (SiO_2/Al_2O_3 of 88.6) showed that it could be reused at least four times with only minor performance loss due to the accumulation of organic residues. Its catalytic performance could be fully recovered by a regeneration treatment involving calcination. The catalyst's crystallinity and structural integrity were maintained throughout the recycling tests and regeneration treatment. Our results show a promising result from screening of zeolites for esterification applications.

CRediT authorship contribution statement

Louise Olsson: Writing – review & editing, Supervision, Methodology, Funding acquisition, Conceptualization. **Oleg Pajalic:** Writing – review & editing, Supervision, Methodology, Funding acquisition, Conceptualization. **Derek Creaser:** Writing – review & editing, Supervision, Methodology, Conceptualization. **Ho Hoang Phuoc:** Writing – review & editing, Supervision, Methodology. **Rawipa Intakul:** Writing – original draft, Methodology, Investigation, Formal analysis, Data curation, Conceptualization.

Declaration of Competing Interest

The authors declare the following financial interests/personal relationships which may be considered as potential competing interests: One co-author (Oleg Pajalic) is employed by Perstorp AB. If there are other authors, they declare that they have no known competing financial interests or personal relationships that could have appeared to influence the work reported in this paper.

Acknowledgements

This work was performed at Chemical Engineering, Competence Centre for Catalysis (KCK) and Centre for Chemical Process Engineering (CPE) at Chalmers University of Technology in collaboration with Perstorp AB. We would like to acknowledge the funding from Swedish Energy Agency (P2021–00082). We also appreciate Dr. Guido de Reijer for his assistance with the pyridine DRIFT experiment. We would also like to acknowledge the usage of characterization instruments at CMAL, Chalmers.

Appendix A. Supporting information

Supplementary data associated with this article can be found in the online version at doi:10.1016/j.apcata.2025.120708.

Data availability

Data will be made available on request.

References

[1] A.S. Sushant M, Eswara P., Glycerol Market by Source (Biodiesel, Fatty Alcohol, Fatty Acid, and Others), Product (Refined Glycerin and Crude Glycerin), and End-use Industry (Personal Care, Food & Beverages, Pharmaceuticals, and Others): Global Opportunity Analysis and Industry Forecast, 2022-2031, Allied Market Report, 2022.
[2] J.-P. Lange, R. Price, P.M. Ayoub, J. Louis, L. Petrus, L. Clarke, H. Gosselink, Valeric biofuels: a platform of cellulosic transportation fuels, Angew. Chem. Int. Ed. 49 (2010) 4479–4483.
[3] I. Dosuna-Rodríguez, E.M. Gaigneaux, Glycerol acetylation catalysed by ion exchange resins, Catal. Today 195 (2012) 14–21.
[4] V.L.C. Gonçalves, B.P. Pinto, J.C. Silva, C.J.A. Mota, Acetylation of glycerol catalyzed by different solid acids, Catal. Today 133-135 (2008) 673–677.
[5] K. Abida, A. Ali, A review on catalytic role of heterogeneous acidic catalysts during glycerol acetylation to yield acetins, J. Indian Chem. Soc. 99 (2022) 100459.
[6] K. Kaur, R.K. Wanchoo, A.P. Toor, Sulfated iron oxide: a proficient catalyst for esterification of butanoic acid with glycerol, Ind. Eng. Chem. Res. 54 (2015) 3285–3292.
[7] K. Kaur, R.K. Wanchoo, A.P. Toor, Enhancement in conversion and selectivity of trivalerin using reactive distillation, Ind. Eng. Chem. Res. 56 (2017) 12488–12494.
[8] D. Singh, P. Patidar, A. Ganesh, S. Mahajani, Esterification of oleic acid with glycerol in the presence of supported zinc oxide as catalyst, Ind. Eng. Chem. Res. 52 (2013) 14776–14786.
[9] I. Díaz, C. Márquez-Alvarez, F. Mohino, Jn Pérez-Pariente, E. Sastre, Combined alkyl and sulfonic acid functionalization of MCM-41-type silica: Part 2. Esterification of glycerol with fatty acids, J. Catal. 193 (2000) 295–302.
[10] K. Lakhya Jyoti, K. Lakhya Jyoti, M.A. Päivi, M.-A. Päivi, K. Narendra, K. Narendra, M. Jyri-Pekka, M. Jyri-Pekka, S. Anil Kumar, S. Anil Kumar, D. Dhanapati, D. Dhanapati, Selective esterification of fatty acids with glycerol to monoglycerides over –SO3H functionalized carbon catalysts, Reaction Kinetics, Mech. Catal. (2016).
[11] M.H.M. Yusoff, A.Z. Abdullah, Catalytic behavior of sulfated zirconia supported on SBA-15 as catalyst in selective glycerol esterification with palmitic acid to monopalmitin, J. Taiwan Inst. Chem. Eng. 60 (2016) 199–204.
[12] Md.S. Machado, J. Pérez-Pariente, E. Sastre, D. Cardoso, A.M. de Guereñu, Selective synthesis of glycerol monolaurate with zeolitic molecular sieves, Appl. Catal. A Gen. 203 (2000) 321–328.
[13] Jn Pérez-Pariente, I. Díaz, F. Mohino, E. Sastre, Selective synthesis of fatty monoglycerides by using functionalised mesoporous catalysts, Appl. Catal. A Gen. 254 (2003) 173–188.
[14] H. Lilis, H. Lilis, H. Lilis, H. Lilis, A. Ahmad Zuhairi, A. Ahmad Zuhairi, M. Abdul Rahman, M. Abdul Rahman, Synthesis of monoglyceride through glycerol esterification with lauric acid over propyl sulfonic acid post-synthesis functionalized SBA-15 mesoporous catalyst, Chem. Eng. J. (2011).
[15] L. Hermida, A.Z. Abdullah, A.R. Mohamed, Synthesis of monoglyceride through glycerol esterification with lauric acid over propyl sulfonic acid post-synthesis functionalized SBA-15 mesoporous catalyst, Chem. Eng. J. 174 (2011) 668–676.
[16] N. Karanwal, D. Verma, P. Butolia, S.M. Kim, J. Kim, One-pot direct conversion of levulinic acid into high-yield valeric acid over a highly stable bimetallic Nb-Cu/Zr-doped porous silica catalyst, Green. Chem. 22 (2020) 766–787.
[17] R. Pothu, R. Gundeboyina, R. Boddula, V. Perugopu, J. Ma, Recent advances in biomass-derived platform chemicals to valeric acid synthesis, N. J. Chem. 46 (2022) 5907–5921.
[18] E. Ramírez, R. Bringué, C. Fité, M. Iborra, J. Tejero, F. Cunill, Assessment of ion exchange resins as catalysts for the direct transformation of fructose into butyl levulinate, Appl. Catal. A Gen. 612 (2021) 117988.
[19] B.O.Dalla Costa, H.P. Decolatti, M.S. Legnoverde, C.A. Querini, Influence of acidic properties of different solid acid catalysts for glycerol acetylation, Catal. Today 289 (2017) 222–230.
[20] P. Ferreira, I.M. Fonseca, A.M. Ramos, J. Vital, J.E. Castanheiro, Esterification of glycerol with acetic acid over dodecamolybdophosphoric acid encaged in USY zeolite, Catal. Commun. 10 (2009) 481–484.
[21] P. Gautam, S. Barman, A. Ali, Catalytic performance of cerium-modified ZSM-5 zeolite as a catalyst for the esterification of glycerol with acetic acid, Int. J. Chem. React. Eng. 18 (2020).
[22] J. Liu, Z. Wang, Y. Sun, R. Jian, P. Jian, D. Wang, Selective synthesis of triacetin from glycerol catalyzed by HZSM-5/MCM-41 micro/mesoporous molecular sieve, Chin. J. Chem. Eng. 27 (2019) 1073–1078.
[23] L. Zhou, E. Al-Zaini, A.A. Adesina, Catalytic characteristics and parameters optimization of the glycerol acetylation over solid acid catalysts, Fuel 103 (2013) 617–625.

[24] F.R. Tentor, D.B. Dias, M.R. Gomes, J.G.P. Vicente, L. Cardozo-Filho, M.E. Berezuk, Glycerol acetylation with propionic acid using iron and cobalt oxides in Al-MCM-41 catalysts 2020 (2020) 16.
[25] S. Wang, J. Pu, J. Wu, H. Liu, H. Xu, X. Li, H. Wang, SO42–/ZrO2 as a solid acid for the esterification of palmitic acid with methanol: effects of the calcination time and recycle method, ACS Omega 5 (2020) 30139–30147.
[26] W. Tang, M. Gao, B. Zhang, X. Wang, C. Wu, Q. Wang, S. Liu, Performance and deactivation mechanism of a carbon-based solid acid catalyst in the esterification of soybean saponin acid oil, J. Environ. Chem. Eng. 11 (2023) 109797.
[27] X. Mo, D.E. López, K. Suwannakarn, Y. Liu, E. Lotero, J.G. Goodwin, C. Lu, Activation and deactivation characteristics of sulfonated carbon catalysts, J. Catal. 254 (2008) 332–338.
[28] K. Suwannakarn, E. Lotero, J.G. Goodwin, C. Lu, Stability of sulfated zirconia and the nature of the catalytically active species in the transesterification of triglycerides, J. Catal. 255 (2008) 279–286.
[29] T. Okuhara, Water-tolerant solid acid catalysts, Chem. Rev. 102 (2002) 3641–3666.
[30] J. Shi, L. Zhang, Z. Cheng, Design of water-tolerant solid acids: a trade-off between hydrophobicity and acid strength and their catalytic performance in esterification, Catal. Surv. Asia 25 (2021) 279–300.
[31] N. Katada, K. Suzuki, T. Noda, G. Sastre, M. Niwa, Correlation between Brønsted acid strength and local structure in zeolites, J. Phys. Chem. C. 113 (2009) 19208–19217.
[32] W.O. Haag, R.M. Lago, P.B. Weisz, The active site of acidic aluminosilicate catalysts, Nature 309 (1984) 589–591.
[33] E.G. Fawaz, D.A. Salam, T.J. Daou, Esterification of linoleic acid using HZSM-5 zeolites with different Si/Al ratios, Microporous Mesoporous Mater. 294 (2020) 109855.
[34] D.M. Dal Pozzo, J.A. Azevedo dos Santos, E.S. Júnior, R.F. Santos, A. Feiden, S. N. Melegari de Souza, I. Burgardt, Free fatty acids esterification catalyzed by acid Faujasite type zeolite, RSC Adv. 9 (2019) 4900–4907.
[35] E.G. Fawaz, D.A. Salam, L. Pinard, T.J. Daou, Study on the catalytic performance of different crystal morphologies of HZSM-5 zeolites for the production of biodiesel: a strategy to increase catalyst effectiveness, Catal. Sci. Technol. 9 (2019) 5456–5471.
[36] R. Zhang, S. Xu, D. Raja, N.B. Khusni, J. Liu, J. Zhang, S. Abdulridha, H. Xiang, S. Jiang, Y. Guan, Y. Jiao, X. Fan, On the effect of mesoporosity of FAU Y zeolites in the liquid-phase catalysis, Microporous Mesoporous Mater. 278 (2019) 297–306.
[37] M. Milina, S. Mitchell, J. Pérez-Ramírez, Prospectives for bio-oil upgrading via esterification over zeolite catalysts, Catal. Today 235 (2014) 176–183.
[38] X.-G. Li, X. Huang, Y.-L. Zhang, H. Li, W.-D. Xiao, Z. Wei, Effect of n-butanol cofeeding on the deactivation of methanol to olefin conversion over high-silica HZSM-5: a mechanism and kinetic study, Chem. Eng. Sci. 226 (2020) 115859.
[39] G.J. Gomes, M.B. Costa, P.R.S. Bittencourt, M.F. Zalazar, P.A. Arroyo, Catalytic improvement of biomass conversion: effect of adding mesoporosity on MOR zeolite for esterification with oleic acid, Renew. Energy 178 (2021) 1–12.
[40] K. Kaur, R.K. Wanchoo, A.P. Toor, Elementary transformation of glycerol to trivalerin: design of an experimental approach, ACS Sustain. Chem. Eng. 5 (2017) 802–808.
[41] S. Brunauer, P.H. Emmett, E. Teller, Adsorption of gases in multimolecular layers, J. Am. Chem. Soc. 60 (1938) 309–319.
[42] G.J.L. de Reijer, A. Schaefer, A. Hellman, P.-A. Carlsson, Catalytic conversion of furans to aromatics over Ga-MFI zeotypes with varying gallium content, Ind. Eng. Chem. Res. 64 (2025) 2025–2035.
[43] C.A. Emeis, Determination of integrated molar extinction coefficients for infrared absorption bands of pyridine adsorbed on solid acid catalysts, J. Catal. 141 (1993) 347–354.
[44] M. Niwa, N. Katada, New method for the temperature- programmed desorption (TPD) of ammonia experiment for characterization of zeolite acidity: a review, Chem. Rec. 13 (2013) 432–455.
[45] H. Hattori, Y. Ono, Solid acid catalysis: from fundamentals to applications, CRC Press, 2015.
[46] B.E. Handyla, A. Jacobo, M.G. Cárdenas Galindo, M. González, M.E. Llanos, M. de Lourdes Gúzman, F. Hernández, Combined thermometric analysis of a series of highly dealuminated USY zeolites, Top. Catal. 19 (2002) 249–258.
[47] C.S. Triantafillidis, A.G. Vlessidis, N.P. Evmiridis, H.−Y. Dealuminated, Zeolites: influence of the degree and the type of dealumination method on the structural and acidic characteristics of H−Y zeolites, Ind. Eng. Chem. Res. 39 (2000) 307–319.
[48] M. Brändle, J. Sauer, Acidity differences between inorganic solids induced by their framework structure. a combined quantum mechanics/molecular mechanics ab initio study on zeolites, J. Am. Chem. Soc. 120 (1998) 1556–1570.
[49] M. Duque-Bernal, J.D. Quintero-Arias, W. Osorio-Viana, I. Dobrosz-Gómez, J. Fontalvo, M.Á. Gómez-García, Kinetic study on the homogeneous esterification of acetic acid with isoamyl alcohol, Int. J. Chem. Kinet. 45 (2013) 10–18.
[50] L. Molinero, M. Ladero, J.J. Tamayo, F. García-Ochoa, Homogeneous catalytic esterification of glycerol with cinnamic and methoxycinnamic acids to cinnamate glycerides in solventless medium: kinetic modeling, Chem. Eng. J. 247 (2014) 174–182.
[51] N. Fattahi, K. Triantafyllidis, R. Luque, A. Ramazani, Zeolite-based catalysts: a valuable approach toward ester bond formation, Catalysts 9 (2019) 758.
[52] P. Prinsen, R. Luque, C. González-Arellano, Zeolite catalyzed palmitic acid esterification, Microporous Mesoporous Mater. 262 (2018) 133–139.
[53] A. Platon, W.J. Thomson, Quantitative Lewis/Brönsted ratios using DRIFTS, Ind. Eng. Chem. Res. 42 (2003) 5988–5992.
[54] S. Morin, P. Ayrault, N.S. Gnep, M. Guisnet, Influence of the framework composition of commerical HFAU zeolites on their activity and selectivity in m-xylene transformation, Appl. Catal. A Gen. 166 (1998) 281–292.
[55] F.E. Imbert, N.S. Gnep, P. Ayrault, M. Guisnet, Effects of commercial HFAU structural parameters over m-cresol transformation, Appl. Catal. A Gen. 215 (2001) 225–234.
[56] M.J. Remy, D. Stanica, G. Poncelet, E.J.P. Feijen, P.J. Grobet, J.A. Martens, P. A. Jacobs, Dealuminated H−Y zeolites: relation between physicochemical properties and catalytic activity in heptane and decane isomerization, J. Phys. Chem. 100 (1996) 12440–12447.
[57] D. Zhai, Y. Liu, H. Zheng, L. Zhao, J. Gao, C. Xu, B. Shen, A first-principles evaluation of the stability, accessibility, and strength of Brønsted acid sites in zeolites, J. Catal. 352 (2017) 627–637.
[58] International Zeolite Association.
[59] D.R. Fernandes, A.S. Rocha, E.F. Mai, C.J.A. Mota, V. Teixeira da Silva, Levulinic acid esterification with ethanol to ethyl levulinate production over solid acid catalysts, Appl. Catal. A Gen. 425-426 (2012) 199–204.
[60] Z. Qin, B. Shen, Z. Yu, F. Deng, L. Zhao, S. Zhou, D. Yuan, X. Gao, B. Wang, H. Zhao, H. Liu, A defect-based strategy for the preparation of mesoporous zeolite Y for high-performance catalytic cracking, J. Catal. 298 (2013) 102–111.
[61] H. An, F. Zhang, Z. Guan, X. Liu, F. Fan, C. Li, Investigating the coke formation mechanism of H-ZSM-5 during methanol dehydration using operando UV–Raman spectroscopy, ACS Catal. 8 (2018) 9207–9215.
[62] A. Zabihpour, J. Ahmadpour, F. Yaripour, Strategies to control reversible and irreversible deactivation of ZSM-5 zeolite during the conversion of methanol to propylene (MTP): A review, Chem. Eng. Sci. 273 (2023) 118639.
[63] M. Díaz, E. Epelde, J. Valecillos, S. Izaddoust, A.T. Aguayo, J. Bilbao, Coke deactivation and regeneration of HZSM-5 zeolite catalysts in the oligomerization of 1-butene, Appl. Catal. B Environ. 291 (2021) 120076.
[64] T. Cordero-Lanzac, A. Ateka, P. Pérez-Uriarte, P. Castaño, A.T. Aguayo, J. Bilbao, Insight into the deactivation and regeneration of HZSM-5 zeolite catalysts in the conversion of dimethyl ether to olefins, Ind. Eng. Chem. Res. 57 (2018) 13689–13702.
[65] M. Guisnet, L. Costa, F.R. Ribeiro, Prevention of zeolite deactivation by coking, J. Mol. Catal. A Chem. 305 (2009) 69–83.
[66] I. Halasz, K. Song, B. Marcus, Hydrophilic and hydrophobic adsorption on Y zeolites, Mol. Phys. 100 (2002) 3123–3132.
[67] A. Osatiashtiani, B. Puértolas, C.C.S. Oliveira, J.C. Manayil, B. Barbero, M. Isaacs, C. Michailof, E. Heracleous, J. Pérez-Ramírez, A.F. Lee, K. Wilson, On the influence of Si:Al ratio and hierarchical porosity of FAU zeolites in solid acid catalysed esterification pretreatment of bio-oil, Biomass. Convers. Biorefinery 7 (2017) 331–342.
[68] S.R. Kirumakki, N. Nagaraju, S. Narayanan, A comparative esterification of benzyl alcohol with acetic acid over zeolites Hβ, HY and HZSM5, Appl. Catal. A Gen. 273 (2004) 1–9.
[69] A.G.M. Ferreira, A.P.V. Egas, I.M.A. Fonseca, A.C. Costa, D.C. Abreu, L.Q. Lobo, The viscosity of glycerol, J. Chem. Thermodyn. 113 (2017) 162–182.
[70] L. Xu, R. Zhao, W. Zhang, One-step high-yield production of renewable propene from bioethanol over composite ZnCeOx oxide and HBeta zeolite with balanced Brönsted/Lewis acidity, Appl. Catal. B Environ. 279 (2020) 119389.